255800-17-F (Vol. II)

Final Report

SAR Imaging via Modern 2-D Spectral Estimation Methods

Volume II: Impact on Automatic Target Recognition

J. M. Gleason
S. I. Stokely
E. R. Keydel

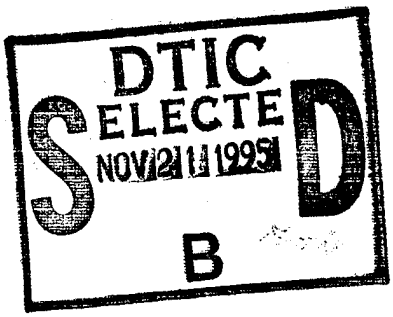

September 1995

Prepared for:
Advanced Research Projects Agency
3701 North Fairfax Drive
Arlington, VA 22203-1714

Contract Number DAAH01-93-C-R178
ARPA Order No. A284

ERIM
P.O. Box 134001
Ann Arbor, MI 48113-4001

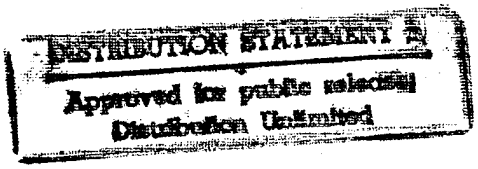

ERIM-320

REPORT DOCUMENTATION PAGE

Form Approved
OMB No. 0704-0188

1. AGENCY USE ONLY (*Leave Blank*)	2. REPORT DATE	3. REPORT TYPE AND DATES COVERED
	September 1995	Final Scientific & Technical Report, 5-94 thru 6-95

4. TITLE AND SUBTITLE

SAR Imaging via Modern 2-D Spectral Estimation Methods
Volume II: Impact on Automatic Target Recognition

5. FUNDING NUMBERS

Phase 1: $184,136
Phase 2: $185,267
Total: $369,403

6. AUTHOR(S)

J.M. Gleason, S.I. Stokely, E.R. Keydel

7. PERFORMING ORGANIZATION NAME(S) AND ADDRESS(ES)

Environmental Research Institute of Michigan
P.O. Box 134001
Ann Arbor, MI 48113-4001

8. PERFORMING ORGANIZATION REPORT NUMBER

255800-17-F (Volume II)

9. SPONSORING/MONITORING AGENCY NAME(S) AND ADDRESS(ES)

Advanced Research Projects Agency
3701 N. Fairfax Drive
Arlington, VA 22203-1714

10. SPONSORING/MONITORING AGENCY REPORT NUMBER

11. SUPPLEMENTARY NOTES

12a. DISTRIBUTION/AVAILABILITY STATEMENT

Approved for public release; distribution unlimited.

12b. DISTRIBUTION CODE

13. ABSTRACT (*Maximum 200 words*)

This report discusses the results of a study to evaluate the impact of several promising adaptive image formation processing (AIFP) methods on the performance of ATR algorithms for fine resolution SAR images of ground-order-of-battle (GOB) targets. The AIFP methods are an extension of modern 2D spectral estimation techniques. Relative to traditional Fourier image formation processing, they offer the potential for improved image resolution, enhanced target-to-clutter contrast, and reduced speckle levels. Three specific AIFP methods were considered: adaptive sidelobe removal, spatially variant apodization, and minimum variance. ATR performance was analysed using a correlation-based target classification algorithm that is representative of state-of-the-art SAR template matching approaches. The results showed that SVA image quality is significantly better than Taylor weighted Fourier image quality for the identical phase history data set. The results also showed that SVA imagery offers the potential for improved target classification performance relative to Taylor weighted Fourier imagery. The simple correlation-based target classification algorithm performed well in separating tanks of diffierent classes from each other and from other confusion target classes.

14. SUBJECT TERMS

Adaptive image formation, 2-D spectral estimation, automatic target recognition, correlation-based target classification

15. NUMBER OF PAGES

64

16. PRICE CODE

17. SECURITY CLASSIFICATION OF REPORT	18. SECURITY CLASSIFICATION OF THIS PAGE	19. SECURITY CLASSIFICATION OF ABSTRACT	20. LIMITATION OF ABSTRACT
UNCLASSIFIED	UNCLASSIFIED	UNCLASSIFIED	

PREFACE

This is *Volume II* of a three volume contract final report, titled, *SAR Imaging via Modern 2-D Spectral Estimation Methods*. *Volume I: Imaging Methods* documents the results of an initial contract study to develop and demonstrate 2-D spectral estimation methods for synthetic aperture radar (SAR) image formation processing. It provides a synopsis of 2-D spectral estimation methods, discusses their relative merits for SAR processing, and illustrates their performance on simulated and collected SAR imagery. The report also develops multi-channel variants of three related methods to estimate scene reflectivity and height from polarimetric, displaced-aperture, interferometric, SAR data.

This volume documents the results of a subsequent study under the same contract. The objective of this latter effort was to quantify the impact of several promising spectral estimation methods on the performance of SAR automatic target recognition (ATR) algorithms. *Volume III* is a classified addendum to *Volume II*. It specifies the resolution of the images used in the ATR study and it contains examples of whole scene images and individual target chips processed using the spectral estimation methods considered under the ATR study.

The contract supporting this work was monitored by Dr. Jonathan Schonfeld, Sensor and Technology Office, Advanced Research Projects Agency (ARPA/STO), and Ms. Barbara Robertson, U.S. Army Missile Command. The 2-D spectral estimation methods for SAR processing were developed by Dr. Stuart DeGraaf. The ERIM Program Manager for the ATR study was Mr. Eric Keydel. Dr. James Gleason was the Project Engineer responsible for all technical activities. Ms. Susan Stokely was a key technical contributor.

CONTENTS

FIGURES

TABLES

1.0 INTRODUCTION

Under the contract effort that preceded the study discussed in this report, several adaptive image formation processing (AIFP) methods were developed and demonstrated for synthetic aperture radar (SAR) imagery [2]. The AIFP methods are an extension of modern 2-D spectral estimation techniques. Relative to traditional Fourier image formation processing, they offer the potential for improved image resolution, enhanced target-to-clutter contrast, and reduced speckle levels. Some AIFP methods are computationally intensive, while others are minimally more complex than traditional Fourier algorithms. The AIFP methods were originally demonstrated on simulated SAR images and on a small number of collected (unclassified) SAR images of ships and urban scenes. The promise shown by those studies lead to the research documented in this report.

This report discusses the results of a subsequent contract study to evaluate the impact of several promising AIFP methods on the performance of ATR algorithms for fine resolution SAR images of ground-order-of-battle (GOB) targets. Three specific AIFP methods were selected for examination: adaptive sidelobe removal (ASR), spatially variant apodization (SVA), and minimum variance method (MVM). These are described in detail in Volume I of this report.

ATR performance was analyzed using a correlation-based target classification algorithm. Target classification performance was addressed, rather than detection algorithm performance, because it was hypothesized that the improved resolution of AIFP images would have the greatest positive impact on classification algorithm performance. The correlation-based classification algorithm was selected as a convenient benchmark because it was easily "tuned" to the characteristics of the various image types (SVA, ASR, etc.).

The fine resolution SAR data used in this study was collected by the Wright Laboratory (WL) - ERIM Data Collection System (DCS) under the ARPA/WL 3-D SAR Program [1]. The resolution of the data and the data itself are classified SECRET. The X-band DCS can collect fully polarimetric and interferometric (3-D) SAR data. All of the results that follow were derived using single polarization imagery (vertical transmit and receive) from one of the two interferometric data channels.

Classification algorithm performance was analyzed following a three step process:

- A database of target chips (small images containing targets) was created for AIFP imagery and traditional Fourier processed imagery.

- A series of correlation trials were performed in which reference images for a specific target class, e.g., T72 tank, were correlated against "independent" match images of targets in the same class and targets in several confusion classes. The correlation scores were used as classification discriminants.

- The results of the correlation trials were analyzed to quantify the impact of the image formation processing algorithms on target classification performance, i.e., separability between the reference target class and the confusion target classes.

The ATR study was divided into two phases. During the first phase, a small database of target chips was generated using nine phase history data sets that had been processed under the 3-D SAR Program. Fourier images were produced both with Taylor weighting and uniform aperture weighting. AIFP images were produced using the SVA, ASR, and MVM algorithms. The five processing algorithms yielded distinctly different target signatures (see the classified addendum). The results of the first phase study were inconclusive, primarily because small aspect angle difference between the targets in the reference and match images had a strong effect on the correlation scores and, thus, tended to obscure the potential benefit of the AIFP methods.

The second phase ATR study utilized a greatly expanded database of target chips (over 7500) to overcome the factors that limited the first phase results. The expanded target chip database covered a finely sampled range of target aspect angles that allowed reference images to be correlated against accurately aligned match images of the same target class. Results from the first phase study indicated that, of the three AIFP methods, the SVA algorithms offered the greatest potential for signature quality improvement. The second phase study thus focused on comparing correlation performance between SVA-processed and Taylor weighted Fourier processed imagery.

The remainder of this report documents the results of the ATR study. Section 2 provides a brief description of the SVA, ASR, and MVM AIFP methods. The first phase results are described in Section 3, and the second phase results are presented in Section 4. Section 5 contains conclusions and recommendations for future activities.

2.0 ADAPTIVE IMAGE FORMATION PROCESSING METHODS

Fourier SAR imaging exploits the Fourier transform pair relationship between signal history measurements and scene reflectivity. Fourier imaging exhibits several drawbacks. First, as the collection aperture is of finite size, the spatial resolution afforded by Fourier imaging is inherently limited. Taylor weighting is typically employed to control impulse response (IPR) peak sidelobes and integrated sidelobe energy. Second, finite resolution leads to the classical coherent imaging speckle phenomenon, which is caused by scintillation of independent, unresolved scattering elements. The classic description of SAR image speckle as "multiplicative noise" stems from the fact that the Fourier transform is not an appropriate estimator for complex circular white Gaussian noise levels which is a common signal history domain model for the scattering from a patch of homogeneous clutter. (The magnitude of the Fourier image is Rayleigh distributed, with mean and standard deviation that are both proportional to the square root of the noise power.) On the other hand, a power spectral density (PSD) estimator is appropriate for estimating noise power. PSD estimators are also appropriate for estimating the scattering intensity of deterministic scatterers.

Modern spectral estimation techniques [2-5] offer attractive alternatives to Fourier SAR imaging. These non-linear techniques offer the promise of improved resolution and contrast, and reduced speckle. Improvements in resolution and reductions in sidelobe artifacts arise through adaptive interference nulling, linear predictive modeling, signal-noise sub-space decomposition, or parametric sinusoidal signal history (point scatterer) modeling. Speckle reduction arises through the signal history domain averaging implicit in PSD image estimation. Contrast improvement arises through signal-noise subspace decomposition or algorithm singularities.

The Fourier transform (FFT) approach and adaptive sidelobe reduction (ASR) AIFP method both produce coherent (complex-valued) spectra. These coherent images represent the outputs of banks of 2-D narrowband filters, where each filter output is tuned to a given spatial location. The FFT represents a bank of fixed narrowband filters, while the ASR method represents a bank of adaptive narrowband filters. The FFT image is a convolution between the scene reflectivity and a space-invariant impulse response. In contrast, the ASR image is a convolution between the scene reflectivity and a space-variant impulse response. The ASR image is computed by applying a space-variant, finite impulse response (FIR) filter to a uniformly weighted (SINC IPR) Fourier image. The ASR filter coefficients are chosen to maximize the output signal-to-interference ratio (SIR) in a single-realization sense. Signal is defined to be the complex sinusoid in the signal history domain that corresponds to a point scatterer at the tuned spatial location, while interference consists of interfering tones, i.e., point scatterers at other locations, together with clutter and noise.

The spatially variant apodization (SVA) AIFP method is a special case of ASR that exhibits minimal impact on clutter. Its dominant effect is to remove the SINC sidelobe artifacts present in unweighted Fourier imagery. SVA exploits a separable ASR filter of order one together with a filter coefficient positivity constraint. This constraint represents the oscillatory nature of a SINC IPR. When the pixel being operated on is a sidelobe of a SINC IPR, the neighboring lags are of opposite sign, and adding them to the input reduces the output energy. An additional ramification of this constraint is that it prevents SVA from sharpening the interpolated SINC mainlobe.

The minimum variance method (MVM) produces a power spectral density (positive semi-definite, real-valued) spectra. PSD images represent the average, or expected value of the output energies of a bank of 2-D narrowband filters, where each filter output is tuned to a given spatial location. MVM represents an adaptive narrowband filter. A correlation matrix, whose entries are an estimate of the correlations between signal history domain data samples, must be estimated from the signal history data. MVM computes narrowband filters that maximize the output SIR in an expected or average sense. It requires a full-rank, nonsingular correlation matrix estimate, which implies a large amount of averaging.

ASR shares the spirit of MVM in that it seeks to maximize SIR. However, it is a "singular" method in that it optimizes SIR on the basis of a unit-rank signal history correlation matrix. Because of this singularity, constraints must be imposed to insure non-zero output. ASR employs a weighting vector constraint. The constraint value controls the behavior of the algorithm. For reasonable choices of the filter order, ASR and SVA methods enjoy a considerable computational advantage over MVM.

3.0 FIRST PHASE STUDY

3.1 TARGET CHIP DATABASE

The database of imagery used in the study was selected from collections of DCS data at the following three sites: Aberdeen Proving Ground, Maryland; Eglin AFB, Florida; and Camp Grayling, Michigan. These collections were chosen because they exhibit a high degree of common targets, aspect angles, and depression angles. Also, phase history data was available from these collections which, as discussed below, was necessary to support certain aspects of the study.

At the outset of the first phase study, this database of images was surveyed to select a subset for an initial ATR sensitivity study. The process of searching for appropriate data was greatly facilitated by an extensive, relational database that had been constructed by ERIM. The database contains detailed information on collected passes, processed data sets, ground truth information, and image truth results.

The database search focused on signature "exemplars" -- targets without camouflage, concealment, and deception (CC&D), in a fixed state of articulation (e.g., tank turrets all pointed in the same direction) at a fixed, nominal depression angle and broadside squint. The parameter range was limited to focus the study on the impact of the AIFP methods rather than performance sensitivity to parameters. The database was queried using the collection and target attributes discussed above, and the query results were ordered by target type, object identification number, aspect angle with respect to the radar illumination, image identification number, and collection.

A set of nine phase histories of the Eglin signature array were selected for use in the initial ATR study. The phase histories were obtained during the first two flights of the Eglin collection. Figure 3-1 shows the ground truth diagram for the Eglin signature array during the time period of the first two flights.

Multiple passes of the Eglin signature array were collected during the first two flights. Among these passes, data was collected along twelve distinct flightlines providing 360 degrees of look-angle coverage at nominal, 30 degree broadside increments. The majority of the imagery was collected at fine resolution at a fixed depression angle of 30 degrees. Although the data was both interferometric and fully polarimetric, the decision was made early in the study to focus on single-channel, non-interferometric data. All of the results that follow (both study phases) were derived

using single polarization (vertical transmit and receive) data from one of the two DCS interferometric channels.

The Eglin signature array contained 15 exemplar targets, placed at variable heading angles in 30 degree increments matched to the direction of the 12 collection passes. This design insured that each target was covered over 360 degrees of aspect angle diversity at a common set of aspect angles. The fifteen exemplar targets included:

- 5 Soviet T72 tanks
- 1 Soviet T62 tank
- 4 U.S. M60 tanks
- 1 2S1 Soviet self-propelled gun
- 2 BMP1 Soviet armored personnel carriers (APCs)
- 1 M113 U.S. APC
- and 1 M35 U.S. cargo truck.

All gun turrets on the tanks were pointed in the forward (firing) direction. Ground truth information for the five T72 tanks and the four M60 tanks did not indicate any significant within-class structural differences. Photographs of the targets showed minor intrinsic variations (e.g., missing fenders) of the type that would be expected from operational military vehicles.

Among the nine phase histories selected for use in this study, four were collected over multiple passes along the same, nominal flightline. These broadside phase histories provided "replicated" images of the signature array, i.e., images from similar, but not identical, look directions.

Whole scene images (2 samples per impulse response width) were produced for the nine phase history data sets with both Taylor (40dB, nbar=5) and uniform aperture weightings. Whole scene SVA and ASR (order, m=2, and constraint, c=0.5) images were produced from the quadratically focused, complex-valued, uniform weighting (i.e., "SINC") images. Using the SINC data, MVM images were produced for selected targets.

Table 3-1 lists the number of exemplar target signatures that were available over the set of nine phase histories. (In this table, 0 degree aspect corresponds to end-on illumination; 90 degree aspect represents broadside illumination from the left.) The aspect angle coverage for each target varied based on its ground heading and the directions of the six distinct flightlines. The specific instance of each target class is denoted by the suffix in the target identification string, e.g., T72-1,

T72-2, T72-3, etc.. The following three aspect angles were selected for consideration during the first phase study: 90, 300, and 330 degrees.

Table 3-1. Target Chips Available for First Phase ATR Study

	Aspect Angles (Degrees)											
Target	**0**	**30**	**60**	**90**	**120**	**150**	**180**	**210**	**240**	**270**	**300**	**330**
T72-1		1	1		1	1	1	4				
T72-2	1	1	1	4						1	1	
T72-3						1	1		1	1	1	4
T72-4						1	1		1	1	1	3
T72-5	1	1		4						1	1	
T62-4	4						1	1		1	1	1
M60-2		1	1	1	4						1	1
M60-3	1	4						1	1		1	1
M60-4						1	1		1	1		4
M60-7				1	1		1	1	1	4		
2S1-1						1	1		1	1	1	2
BMP1-1			2						1	1		1
BMP1-2				1	1		1	1	1	4		
M113-1	1	1	1	4						1	1	
M35-1				1	1		1	1	1	4		

Target chips at the selected aspect angles were extracted from the SINC, Taylor weighted (TW), SVA, and ASR whole scene images using image truth information obtained from the 3-D SAR database. MVM target chips were generated for each target and aspect angle. All of the target chips were magnitude detected.

The classified addendum to this report contains example whole scene images, as well as individual target chips, for each of the five data types. The whole scene MVM image was produced by processing multiple, overlapping patches covering the entire scene.

3.2 CORRELATION TRIALS

The correlation-based target classification algorithm is illustrated in Figure 3-2. A reference image, representing a specific target class, e.g., T72 tank, is correlated against a larger match image, representing a target whose class is unknown, e.g., T72 tank, M60 tank, M35 truck, etc. The sliding window correlation operation computes a normalized correlation coefficient at each location where the reference image fits within the match image. The normalized correlation coefficient, ρ, is computed as shown in the figure, where r represents the reference image pixels and m represents the match image pixels corresponding to one translation of the reference image. The ensemble expected values indicated in the figure are computed as averages over the available sample set. The reference images used in this effort were typically 60 x 60 pixels and the match images were typically 100 x 100 pixels, resulting in 41 x 41 sample correlation arrays. The peak extraction operation shown in Figure 3-2 returns the value of the correlation peak, ρ_{max}, and its location in the full correlation array.

During the first phase study, correlation trials were executed for many combinations of reference and match images. Table 3-2 summarizes the trials for the T72 tank at 90 degree aspect angle. The trials listed in the table were repeated for each of the five image types. As shown in Table 3-1, 90 degree aspect angle target chips of the T72 tank were available for two specific instances: T72-2 and T72-5. These two targets had the same nominal, ground heading angle. Images of T72-2 showed a prominent glint from the gun barrel; images of T72-5 did not show the gun barrel glint indicating that either the target or the turret was most likely rotated by a few degrees with respect to T72-2. Four "looks" were available for T72-2 and T72-5 (as listed in Table 3-1); the looks were obtained from the four replicated passes along the same, nominal flightline. The images for the individual tank instances did not show any apparent rotation among the replicated looks, although minor variations were evident in the signatures.

As shown in Table 3-2, classification performance was investigated for three types of reference images: single look (SL), look-averaged (LA), and within-class and look-averaged (WC&LA). The eight SL references were obtained using T72 target chips from the images produced for the flights and passes listed in the table (e.g., e103 corresponds to data collected along flight 1, pass 3). Each of the eight 60 x 60 pixel SL references were approximately centered on the target in the corresponding 100 x 100 pixel target chip.

Table 3-2. T72 Tank Correlation Trials at 90 Degree Aspect Angle

			Match Target and Image							
			T72-2				T72-5			
Ref. Type	Target	Image(s)	e103	e106	e201	e203	e103	e106	e201	e203
Single Look	T72-2	e103	NA	#	#	#	#	#	#	#
		e106		NA	#	#	#	#	#	#
		e201			NA	#	#	#	#	#
		e203				NA	#	#	#	#
	T72-5	e103					NA	#	#	#
		e106						NA	#	#
		e201							NA	#
		e203								NA
Look Averaged	T72-2	e106,e201,e203	#	NA	NA	NA	#	#	#	#
		e103,e201,e203	NA	#	NA	NA	#	#	#	#
		e103,e106,e203	NA	NA	#	NA	#	#	#	#
		e103,e106,e201	NA	NA	NA	#	#	#	#	#
	T72-5	e106,e201,e203	#	#	#	#	#	NA	NA	NA
		e103,e201,e203	#	#	#	#	NA	#	NA	NA
		e103,e106,e203	#	#	#	#	NA	NA	#	NA
		e103,e106,e201	#	#	#	#	NA	NA	NA	#
Within Class & Look Averaged	T72-2,5	e106,e201,e203	#	NA	NA	NA	#	NA	NA	NA
		e103,e201,e203	NA	#	NA	NA	NA	#	NA	NA
		e103,e106,e203	NA	NA	#	NA	NA	NA	#	NA
		e103,e106,e201	NA	NA	NA	#	NA	NA	NA	#

The SL references were correlated against the match targets and images marked by the # symbol in the table. For example, the T72-2 e103 reference was correlated against three T72-2 chips (from e106, e201, and e203), and the four T72-5 chips. The SL references were not correlated against the larger (100 x 100 pixel) target chip from which they were extracted, as indicated by the NA (not applicable) in the table. (It was verified that these correlation operations yielded a value of unity, as would be expected.) The T72-2 reference from image e106 was correlated against the T72-2 match chips from images e201 and e203. It was not correlated against the T72-2 match chip from e103 because that result would be virtually the same as that obtained by correlating the T72-2 reference from e103 against the T72-2 match chip from e106. Similarly, the four T72-2 SL references were correlated against the four T72-5 match chips, but the T72-5 SL references were not correlated against the T72-2 match chips.

The eight LA references were each constructed from three, registered looks at the specific T72 tank (T72-2 or T72-5). As mentioned above, the four looks represented virtually identical aspect angles. The multiple looks at each of the two T72 tanks were registered by cross-correlating among them and translating until they were aligned to the nearest pixel. The table lists the specific target chips used in each LA reference. It shows that the LA references were correlated against the match target chip that was not included in the construction of the reference. Each of the four T72-2

LA references were correlated against the four T72-5 match images. Likewise, the T72-5 LA references were correlated against the one T72-5 image not included in the reference as well as the four T72-2 match images.

The T72 WC&LA references were constructed by averaging six registered T72 target chips -- three for the T72-2 and three for the T72-5. Once again, the registration was performed by cross-correlating among the target chips and shifting each until the correlation peaks were aligned. Each of the four WC&LA references were correlated against the individual T72-2 and T72-5 match images that were not included in the reference.

Although not shown in the table, all of the T72 references were correlated against the eight 90 degree aspect angle confusion targets listed in Table 3-1. They were not correlated against match images at other aspect angles.

Additional correlation trials were conducted using analogous T72 tank references at 300 and 330 degree aspect angles. The analysis results for these references were consistent with the results obtained for the 90 degree aspect angle cases.

3.3 ANALYSIS RESULTS

Analysis results for the within-class and look-averaged (WC&LA) references were generated first, followed successively by results for the look-averaged (LA) references, and the single-look (SL) references. Figure 3-3 shows a histogram of the SINC correlation scores for the four WC&LA references. Eight T72 scores are plotted for the two T72 match images excluded from each of the four references. Among the confusion targets, four scores are shown for the one BMP1 match image and for the one M35 match image. Eight scores are shown for the two M60 match images (M60-2 and M60-7). Sixteen scores are shown for the one M113 APC which had the same nominal ground heading as the T72-2 and T72-5 tanks, yielding four looks from the replicated flightlines. Figures 3-4 through 3-7 show corresponding results for the TW, SVA, ASR and MVM references.

The five plots for the WC&LA references show over the limited T72 sample set examined, that the T72 tanks can be separated from the confusion targets without error in each case by setting an appropriate threshold on the correlation scores.

Figures 3-3 and 3-4 show that the T72 tanks appear to be better separated from the confusion targets in the TW imagery than they are in the SINC imagery. This is expected given the reduced sidelobe levels of the TW imagery. Since the small number of samples from the T72 and confusion target distributions do not overlap in either case, the observation that the T72s are better separated in the TW imagery is subjective, although it is adequate for an initial assessment.

Figure 3-5 shows that the SVA correlation scores for the T72 match images are lower than the comparable TW scores in Figure 3-4 but, more importantly, it shows an improvement in the separability between the T72 tanks and the confusion targets. Figure 3-6 shows that the ASR correlation scores for the T72 match images are even lower than the SVA scores, but that the separability with respect to the confusion targets is approximately the same. The lower T72 correlation scores for the SVA and ASR images, relative to those for the TW images, are a direct consequence of the increased sharpness of the AIFP images. The sharpness of the imagery has the effect of tuning the correlation much more finely to the specifics of the signature content. Even small mismatches (to be expected with different targets) cause a significant reduction in correlation score.

Figure 3-7 shows that the T72 correlation scores for the MVM match images, which are smoother than any of the other data types, are very high, but that the separability of the confusion targets is not as good as it is for the SVA and ASR images.

Figures 3-8 through 3-10 show TW, SVA, and ASR correlation scores for the eight LA references. In these plots, the T72 results are subdivided into two classes. The same-instance (SI) scores are ones in which the eight LA references are matched against independent looks at the same target instance, e.g., a T72-2 reference against a T72-2 match image. The cross-instance (CI) scores are ones in which the eight LA references are correlated against the four match images of the other T72 tank, e.g., a T72-2 reference against a T72-5 match image. Each plot contains eight T72-SI correlation scores and thirty-two T72-CI scores.

Figures 3-8 through 3-10 show that the T72-SI correlation scores are considerably higher than the T72-CI scores. Separability between the same-instance T72s and the confusion targets remains perfect for the small set of samples. For the TW and SVA imagery, the T72-CI scores overlap slightly with the confusion target scores. This can be attributed to two factors which degrade the within-class correlation scores. The first is structural variability between different instances of the same class. The second is small angle misregistration between the signatures. Both of these effects cause signature mismatches between the target instances.

For the ASR imagery, the overlap is considerable. The signature sharpening achieved with ASR accentuates the impact of the above-mentioned signature mismatch on the within-class correlation scores.

Figures 3-11 through 3-13 show corresponding results for the SL references. In these cases, the T72-CI scores overlap considerably with the confusion targets in the TW imagery and the SVA imagery. For the ASR data, even the T72-SI scores partially overlap with the confusion targets. The results show that the T72-SI scores for the SL references are not as well separated from the confusion targets as they are for the LA references. The loss of separability is primarily due to factors identified above. For example, the T72-SI SVA correlation scores for the LA references (Figure 3-9) range from 0.68 to 0.86; the corresponding scores for the SL references (Figure 3-12) vary from 0.60 to 0.88.

The WC&LA references yielded improved performance for the SVA and ASR images, relative to the results for the TW images, because the references were developed based on looks at the same target instances included in the match images. The lower T72-CI scores for the LA references, in comparison to the T72-SI scores, are due, in part, to the small difference in aspect angles between the two tanks, as noted previously. They are also due, in part, to intrinsic, within-class differences between the T72-2 and T72-5 tanks. Intrinsic differences in target structure, due to manufacturing inconsistencies and the normal effects of use and repair, will cause signature variations among multiple instances of the same target class imaged in identical backgrounds from identical collection geometries.

The variability among the T72-SI scores for the SL references is due to two factors -- radar system noise and small differences in target aspect angle among the four replicated images. Radar system noise will cause signature variations among different looks at the same target imaged in identical backgrounds from identical collection geometries. Although visual examination of the replicated looks did not reveal any apparent aspect angle variations, small aspect differences are certainly present.

3.4 SIGNATURE ALIGNMENT STUDIES

As discussed above, one of the conclusions emerging from the first phase study was that signature mismatch due to both small angle variation and within-class variability had a significant impact on

the correlation results. Two simple experiments were conducted near the end of the first phase effort to better understand the impact of intrinsic target variations and small differences between the reference and match image aspect angles.

The precise locations of two corner reflectors in the Eglin signature array were measured in each of the four replicated looks from the same nominal flightline. The two locations established a baseline from which relative rotations among the images were determined. The results, presented in Table 3-3, indicate that the aspect angles between paired looks at the same target instance varied from approximately 0.1 degrees (between the images from passes e106 and e203) to a maximum of approximately 1.1 degrees (between e103 and e106). Visual examination of the data showed that chips of the same target from the closely aligned images were more similar in appearance than were chips from the less accurately aligned images.

Table 3-3. Relative Rotations Among Four Replicated Images

Pass	Measured Angle Relative to Pass e103 (Degrees)
e106	-1.14
e201	-0.61
e203	-1.03

Figure 3-14 shows correlation scores for the T72-2 and T72-5 SL references as a function of the measured reference and match image aspect angle differences. The twelve samples for each data type represent the results of correlating the T72-2 and T72-5 SL reference and match images for the six permutations of the four replicated images. The figure shows that much of the variability in the T72-SI SL correlation scores are "explained" by the small aspect angle differences among the four replicated images. Aspect angle differences as small as 1.1 degrees have significant impact on the correlation scores.

The correlation scores for the reference and match images separated in aspect by 0.1 degrees provide good estimates of the maximum values that should be expected given the presence of radar system noise. The observed sensor "noise ceiling" is 0.93 for TW imagery, 0.88 for SVA imagery, and 0.85 for ASR imagery. The lower noise ceiling values for the SVA and ASR imagery result from the fact that the increased sharpness of the AIFP data accentuates the impact of this noise ceiling on the correlator output.

A second experiment involved processing of additional phase history data sets for one of the four replicated passes. Figure 3-15 illustrates the geometry of phase history data acquisition for SAR image formation. Continuous data is collected over a region that is wider than required to form nominal resolution images. Subset pulse sets are selected to form the image at the nominal resolution. The availability of the extended pulse sequence makes it possible to generate image sequences which are closely spaced in angle. These correspond to different squint angles relative to the scene center.

TW, SVA and ASR images were generated over squint angles from 89.5 to 93.0 degrees in 0.5 degree increments. The limits on the squint angle range were imposed by the amount of phase history data in the original "cut" used to form the broadside image under the 3-D SAR Program. SL references for the T72-2 tank were correlated against T72-5 match chips from the eight images, representing a total of 4.5 degrees of aspect angle variability. The target aspect angle variability resulted from the changing look directions of the squinted images.

The results for each data type showed a correlation "peak" (over the range of squint angle images) when matching the T72-2 and the T72-5 with an aspect angle offset of 3 degrees. This derived estimate of the difference in target aspect angles was consistent with visual examination of the multiple squinted images. The peak correlation scores for the TW, SVA, and ASR images were 0.78, 0.69, and 0.51, respectively, which are well below the noise ceilings discussed above. This difference is a result of within-class target variability, the results of which are emphasized by the AIFP methods As expected, the cross-instance correlation scores fell off rapidly from the peak values.

In summary, the results of the first phase ATR study were inconclusive as to the impact of AIFP methods on the performance of SAR target classification algorithms. The correlation results derived for the nine phase history data sets and the results of the two subsequent experiments showed that the potential benefit of the AIFP methods could easily be masked by the effect of small aspect angle differences between the reference images and the match images of the same target class. The correlation results also showed that a meaningful assessment of classification performance benefits requires that the target references be derived for target instances other than those included in the match image set.

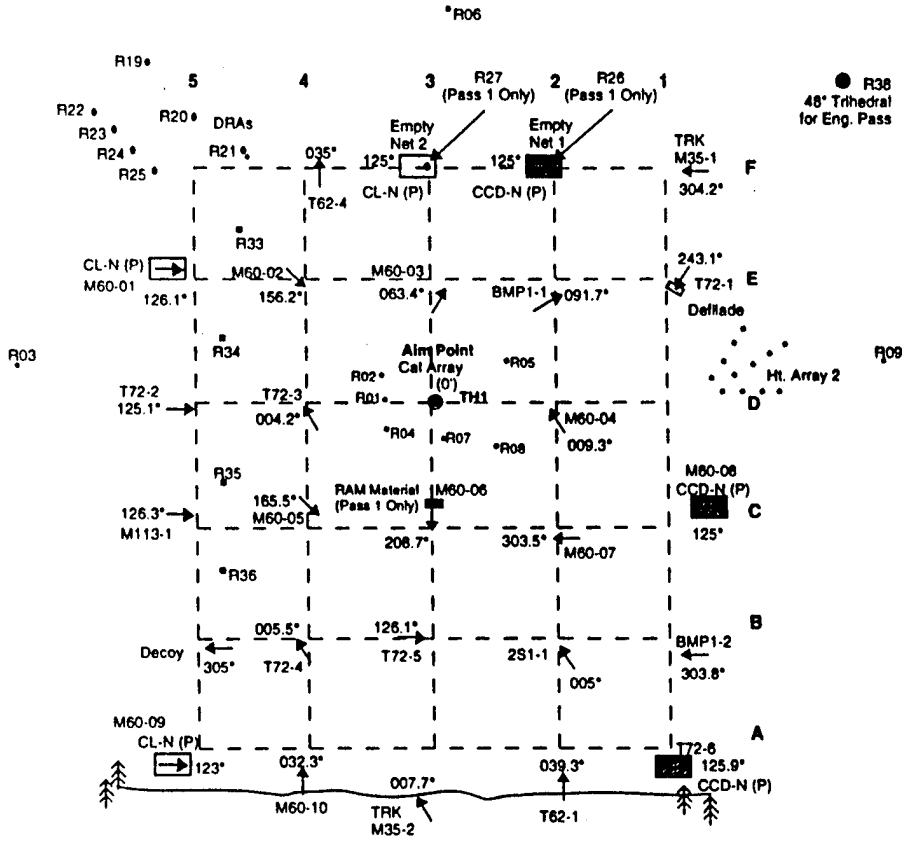

Figure 3-1. Eglin Signature Array Ground Truth Diagram for Flights 1 and 2

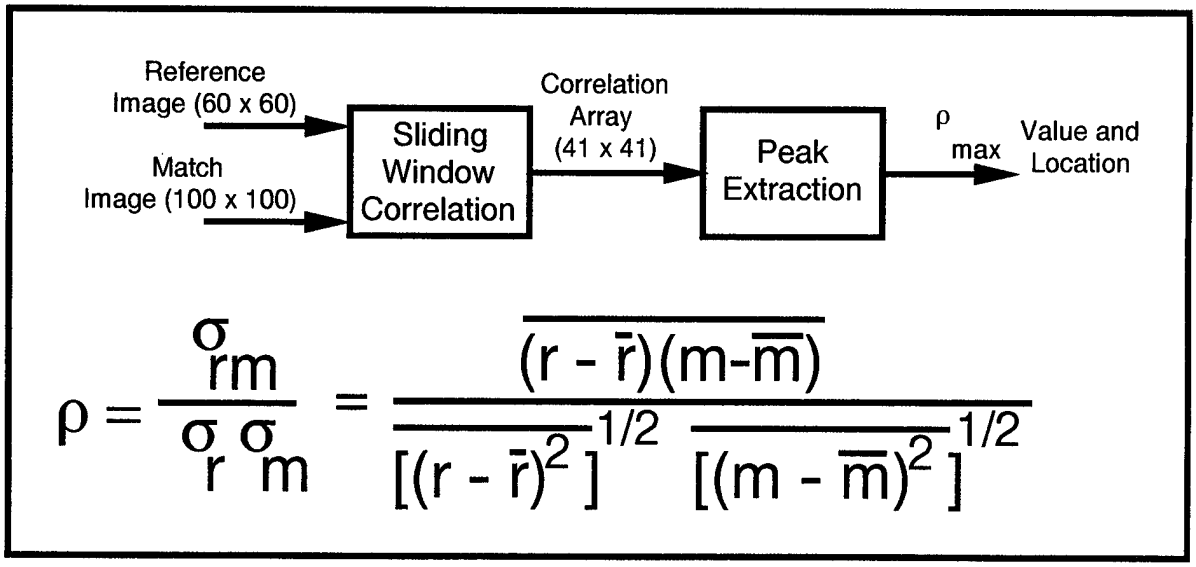

Figure 3-2. Correlation-Based Classification Algorithm

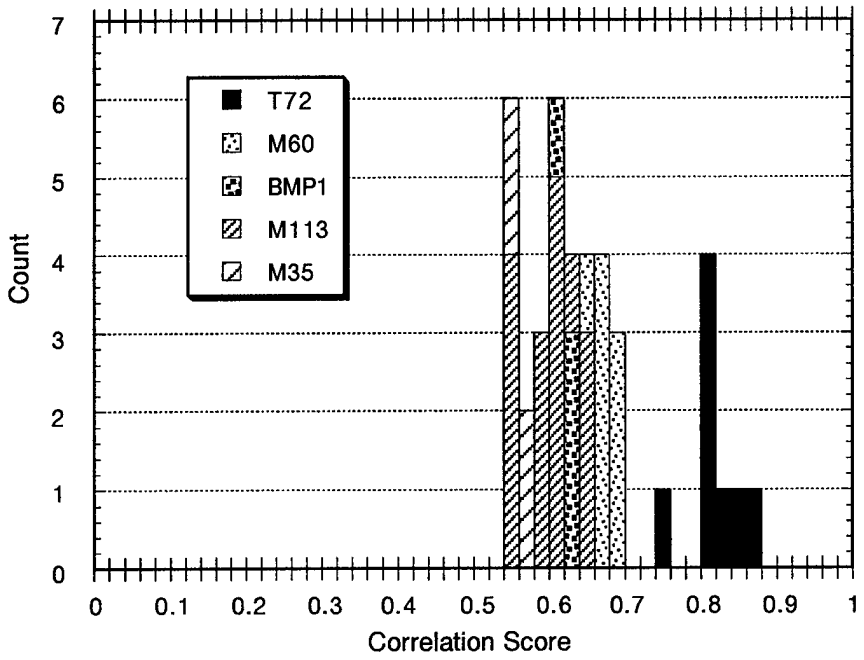

Figure 3-3. SINC Correlation Scores for 90 Degree T72 Within-Class and Look-Averaged References

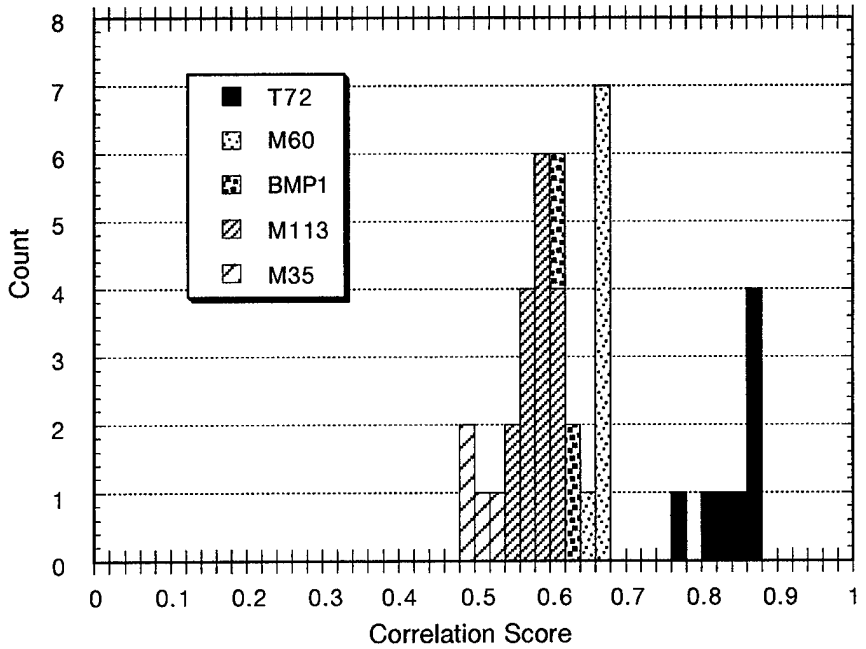

Figure 3-4. TW Correlation Scores for 90 Degree T72 Within-Class and Look-Averaged References

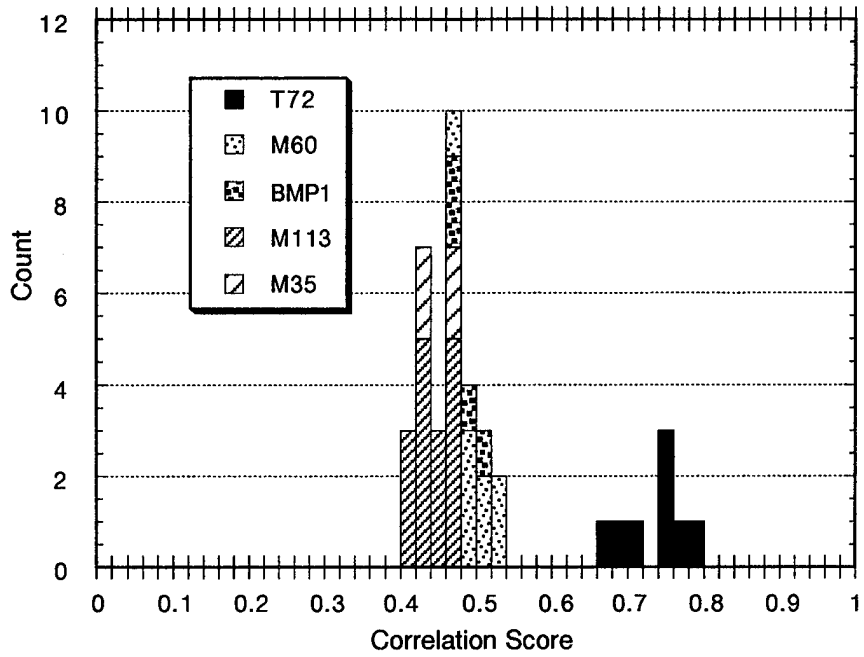

Figure 3-5. SVA Correlation Scores for 90 Degree T72 Within-Class and Look-Averaged References

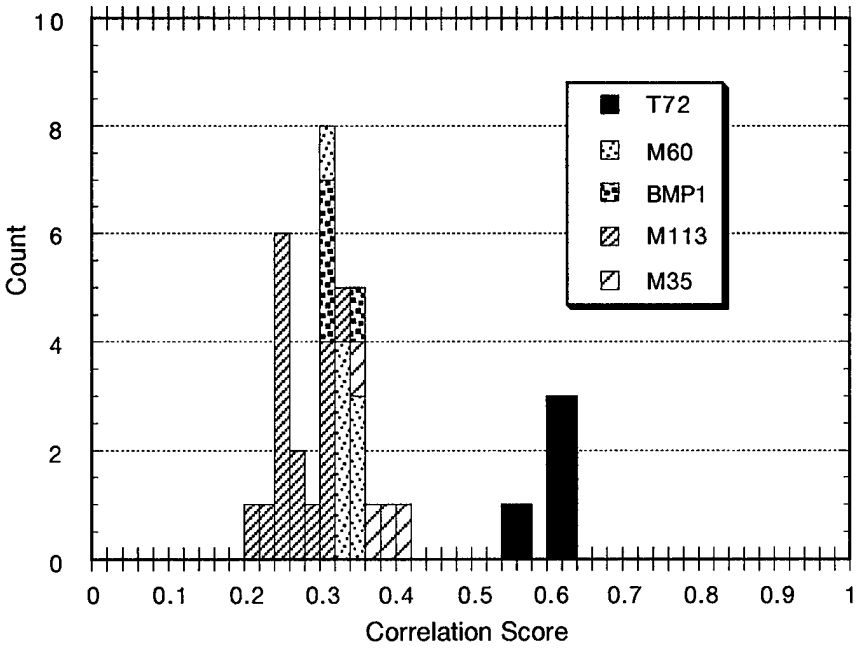

Figure 3-6. ASR Correlation Scores for 90 Degree T72 Within-Class and Look-Averaged References

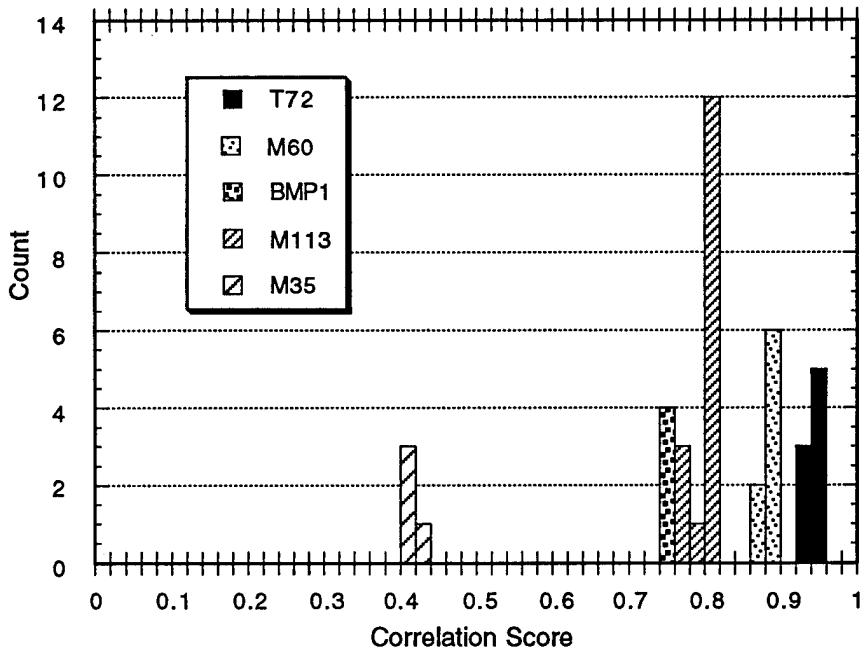

Figure 3-7. MVM Correlation Scores for 90 Degree T72 Within-Class and Look-Averaged References

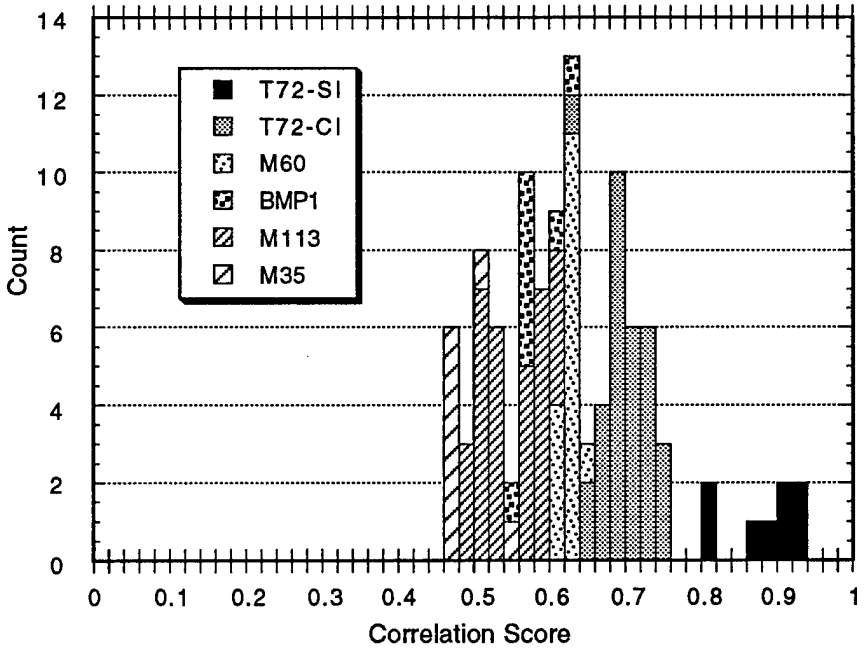

Figure 3-8. TW Correlation Scores for T72 Look-Averaged References

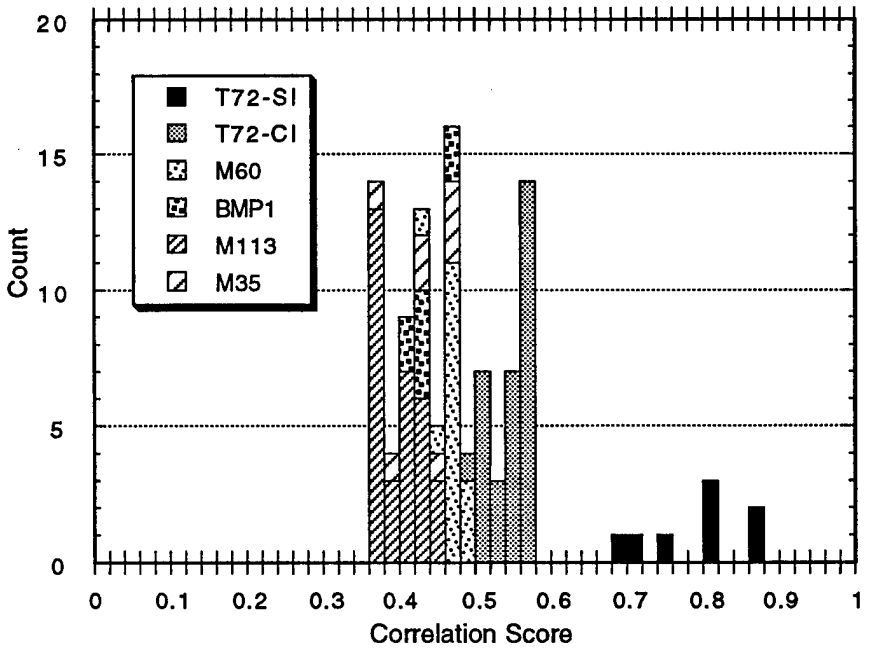

Figure 3-9. SVA Correlation Scores for T72 Look-Averaged References

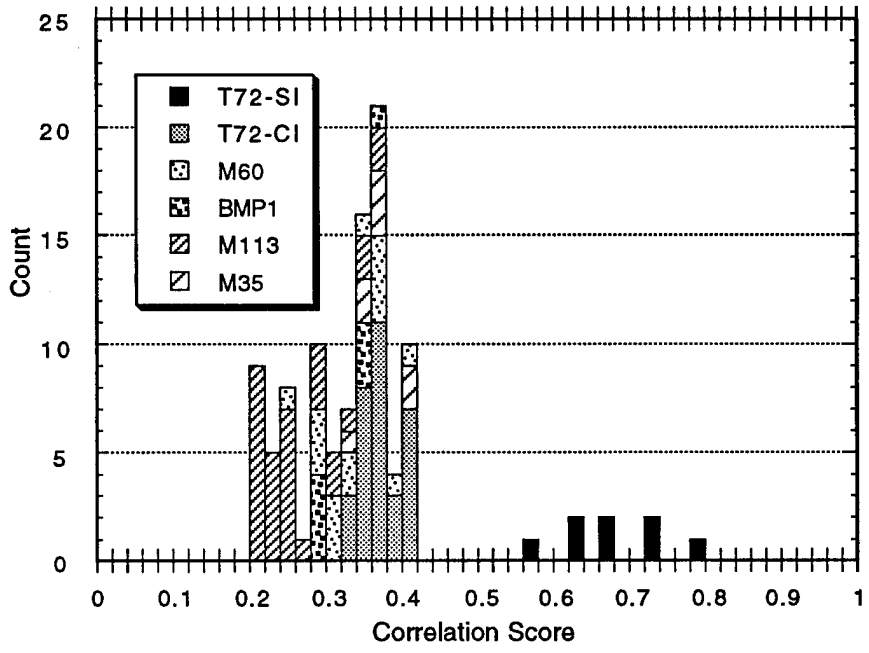

Figure 3-10. ASR Correlation Scores for T72 Look-Averaged References

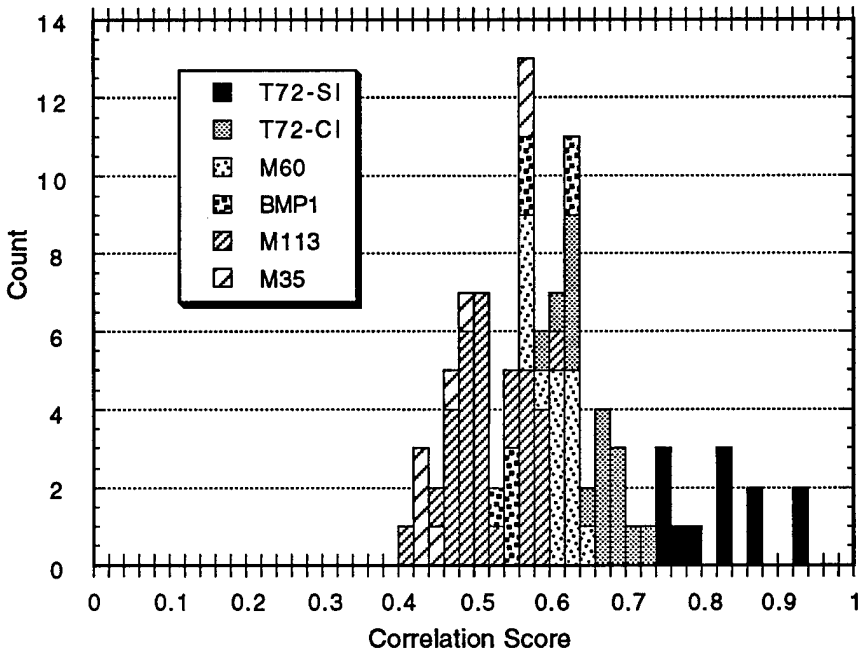

Figure 3-11. TW Correlation Scores for T72 Single-Look References

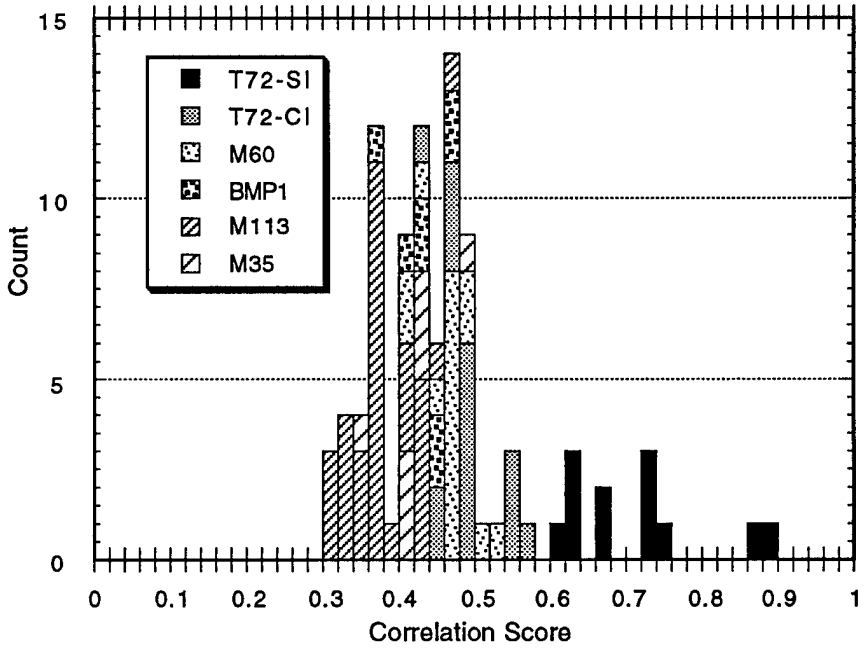

Figure 3-12. SVA Correlation Scores for T72 Single-Look References

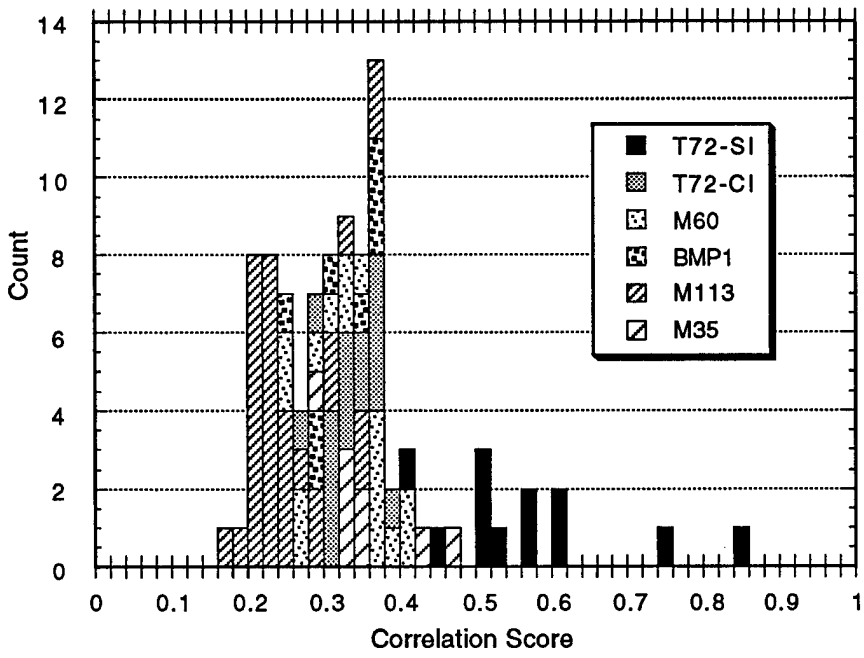

Figure 3-13. ASR Correlation Scores for T72 Single-Look References

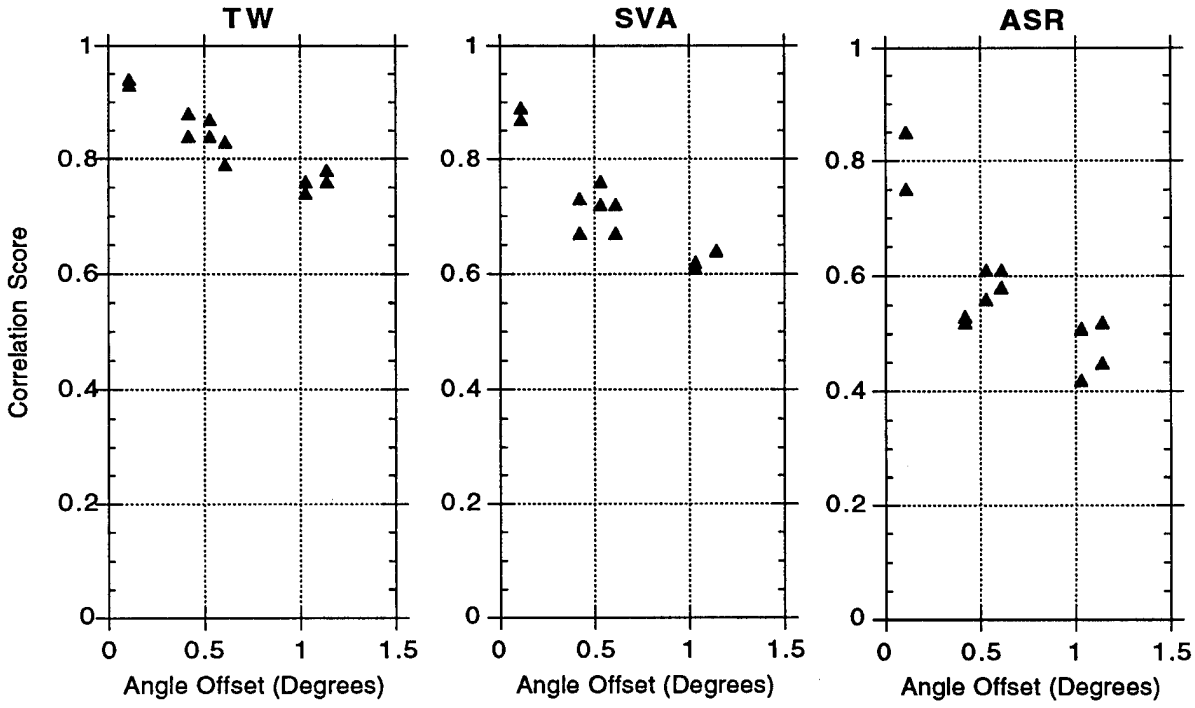

Figure 3-14. TW, SVA, and ASR Correlation Scores for T72-2 and T72-5 Single-Look References as a Function of Reference and Match Aspect Angle Differences

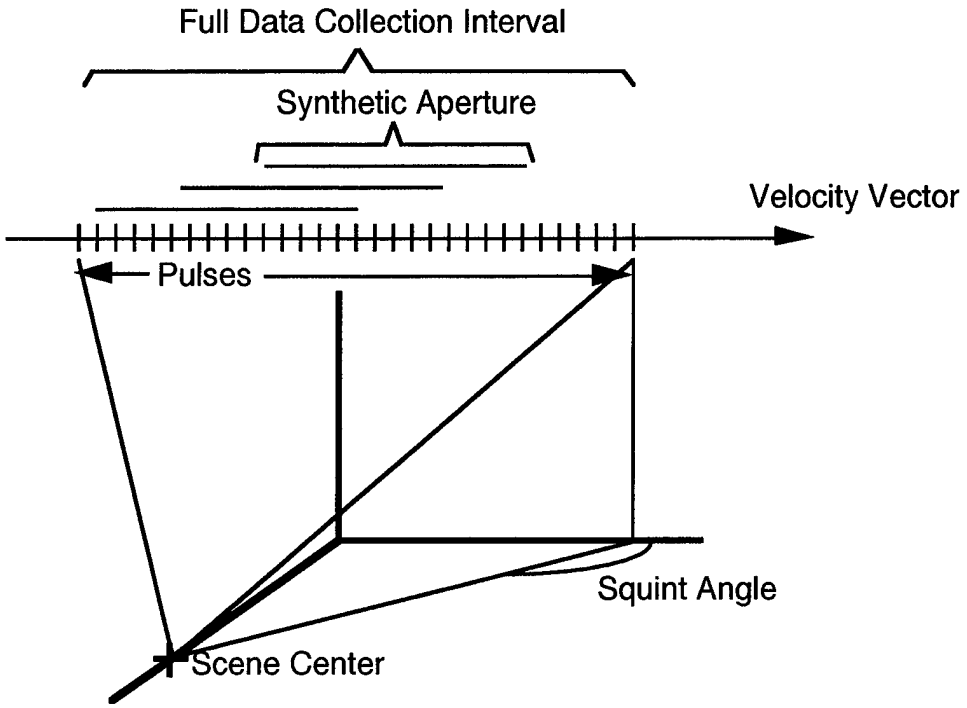

Figure 3-15. Illustration of Data Collection Geometry

4.0 SECOND PHASE STUDY

4.1 EXPANDED TARGET CHIP DATABASE

The second phase ATR study was structured to address the specific factors that caused the first phase results to be inconclusive. An expanded database of target chips was generated for use as reference and match images. Based on initial observations under the first phase study that SVA showed the greatest promise among the three AIFP methods, it was decided to focus the second phase study on a comparison of classification performance for SVA imagery and Taylor weighted (TW) Fourier-processed imagery.

The expanded target chip database was obtained by generating Taylor weighted (TW) and SVA images from phase history over twelve DCS passes of the Eglin signature array, six of which were included in the first phase study. The twelve passes were chosen to provide complete 360 degree coverage of the array in nominal 30 degree look angle increments. All of the passes were collected to provide nominal 30 degree depression angle at broadside squint.. By processing data from the 12 passes providing 360 degree coverage of the Eglin signature array, a complete set of target chips was available for all 15 of the target exemplars listed in Section 3.1.

The spotlight-mode phase history data collected along each pass was processed into images at 21 squint angles, covering ±5 degrees about broadside in 0.5 degree increments. The squinted images along each pass allowed extracted target chips to be aligned in aspect angle to an accuracy of ±0.25 degrees, provided that their precise aspect angles fell within ±5 degrees of the nominal values.

The squinted images along each pass provided target signatures at small angle deviations from their nominal aspect angles. For squint angles within five degrees of broadside, the resulting signature variations with aspect angle are an excellent approximation to the variations that would be obtained by slight changes in the target heading, holding the squint angle at broadside. The precise target aspect angles differ from the nominal values obtained from the ground truth due to slight errors in the flightline directions and slightly larger errors in the target ground headings.

During the first phase study, the TW and SINC images were generated in separate image formation steps. The SVA and ASR images were then derived from the SINC image. Logic incorporated into the DCS image formation processor caused it to use slightly different phase history samples in

producing the TW and SINC images. Thus, there were other sources of differences between the TW and ASR/SVA samples compared in that first phase study.

To remove any possible influence of different phase history sequences for the second phase effort, the image formation processor was run once to generate the SINC image. The processor was set-up to produce the unweighted image by Fourier transforming a phase history data set that was the same size as the output image. The SINC image was then up-sampled by a factor of two by zero-padding and Fourier transforming. The Taylor weighted (40 dB, nbar=5) image and the SVA image were obtained from the up-sampled SINC image. SVA quality is optimized for images that are upsampled by an integer factor. The processing used in the second phase effort insured that the images were upsampled by a precise factor of two. Corner reflector measurements showed that the mainlobe impulse response (IPR) widths of the SVA images were approximately 25% finer than those of the TW images.

A total of 504 full-scene images were generated, corresponding to 12 passes, 21 images per pass, 2 processing algorithms per image (TW and SVA). 7560 target chips (100 x 100 pixels) were automatically extracted from the magnitude detected images: 15 exemplar targets from 540 images. As in the first phase study, all of the images used in the second phase effort were derived from single polarization (vertical transmit and receive) phase histories from one of the two DCS interferometric data channels.

4.2 CORRELATION TRIALS

The impact of TW and SVA processing on target classification performance was investigated using the same correlation-based classification algorithm employed during the first phase ATR study. Correlation scores between targets of the same class and targets of different classes (confusers) were used as discriminant measures. As in the first phase, each correlation trial involved a reference image and a match image. All of the reference images were extracted from single target chips (i.e., they were single-look references). The reference and match images were the same size as those used in the first phase effort. Normalized correlation scores were computed at each location for which the reference image fit within a given match image. The peak value over the resultant correlation array was obtained as the score for that specific trial.

Correlation trials were generated for reference images of two T72 Soviet tanks (T72-2 and T72-3) and one M60 U.S. tank (M60-3). Individual reference images were selected for these three targets

at each of the 12 nominal aspect angles. Each reference image was selected from among the 21 target chips representing small aspect angle deviants about the nominal value. For the cardinal aspect angles (0, 90, 180, and 270 degrees), the reference images were selected after examination of the target chips to be as near as possible to the desired end-on, side-on, and head-on aspect angles. For the 8 non-cardinal aspect angles, the reference target images were selected, among the small aspect angle deviants, as the broadside image.

Each of the selected reference images was correlated against all of the match images at the corresponding aspect angle for the remaining 14 targets. For example, the T72-2 references were cross-correlated against four T72s (T72-1, T72-3, T72-4, and T72-5) and ten confusion targets. All correlation operations were performed using reference and match images of the same data type, i.e., TW references were correlated against TW match images and SVA references were correlated against SVA match images.

A total of 7056 correlation trials were performed for the T72-2 reference images: 14 targets, 12 nominal aspect angles, 21 small aspect angle variations, and 2 image formation algorithms. Over 21,000 correlation operations were performed for the three reference targets.

4.3 ANALYSIS RESULTS

Figure 4-1 shows scores obtained by correlating T72-2 references against T72-1 TW match images over all aspect angles. The straight lines between the scores at successive thirty degree nominal aspect angle increments represent the twenty degree gaps for which correlation scores were not available. As discussed above, the results in Figure 4-1 were obtained using different T72-2 reference images for each of the twelve nominal aspect angles.

Figure 4-1 illustrates the significant degree to which the correlation scores are affected by small differences between the aspect angles of the reference and match image targets. Note the correlation peaks at 90, 180, and 270 degrees. The strength of these correlation peaks is a strong function of the high amplitude and distinctive shape of the signatures. Note the rapid fall-off of the correlation scores with even small reference/match signature angle offsets.

Figure 4-1 also illustrates the significant variation in peak correlation scores (over the 21 small aspect angle increments) at the twelve nominal aspect angles. The peak scores vary from 0.88 at 0 degrees (end-on) to less than 0.65 at 210 degrees. Although the correlation scores are normalized,

they are affected by the spatial and intensity distributions of the reference and match images. The high correlation scores at 0 degree aspect result from the spatially compact, high intensities of the end-on T72-2 signature (see the classified addendum).

The local maxima at the other aspects are less distinct and exhibit noise-like local fluctuation with aspect. The reason for this is that the target signatures are neither as bright nor as well defined in edge boundary as they are at the cardinal angles. The fuzziness of the edge leads to the apparent fluctuations in correlation score within the 2.5 degree aspect range about the indicated aspects.

Figure 4-2 shows corresponding results for the SVA reference and match images. At each aspect angle, the SVA correlation scores are lower than the TW scores, with a typical difference of approximately 0.1. The lower scores for the SVA imagery are attributable to its increased sharpness in comparison to the TW imagery. Figures 4-1 and 4-2 illustrate the high degree to which the SVA scores "track" the TW scores as a function of aspect angle. The decrease in SVA correlation scores relative to the TW results appears to be dominated by the effects of signature mismatch due to within-class variability coupled with the signature sharpness properties of the SVA method.

Figures 4-3 and 4-4 exemplify the difference in small angle aspect sensitivity between the cardinal and off-cardinal angles. The 90 degree case shown in Figure 4-3 degrades significantly with small aspect mismatch due to the strength and sharpness of the signatures. At 120 degrees (Figure 4-4) the sensitivity is much lower due to the fact that the signature edges are less distinct. There does not appear to be a significant increase in aspect sensitivity of the SVA imagery over the TW imagery.

Figures 4-5 and 4-6 show T72-2 correlation scores for T72-2 TW and SVA match images near 90 and 120 degree aspect angles, respectively. These are the only results that will be presented for same-instance reference and match images. The correlation scores are plotted as a function of the squint angle of the match images since that is the parameter by which the reference and match images differ. Both figures show that the scores for the auto-correlation case reach unity, as expected. For the 90 degree nominal aspect angle, the correlation scores peak at 90.5 degree squint angle, corresponding to the specific image from which the T72-2 reference was obtained. The figures show that the SVA correlation values fall off more rapidly from the peak value, as the reference and match target aspect angle difference increases. This is primarily due to the fact that the SVA correlation scores fall to lower values, compared to the TW scores, as the aspect angle difference between the reference and match image increases at the extreme squint angles. The

figures show that the correlation scores fall to lower values for the 90 degree nominal aspect angle than they do for the 120 degree case. This trend is attributable to the more definite structure of the broadside target signature.

Figures 4-7 and 4-8 are comparable to Figures 4-1 and 4-2, except they show T72-2 correlation scores for matches images of a different T72 tank instance (T72-3). In general, the results for the T72-3 match images are similar to those for the T72-1 images (Figures 4-1 and 4-2). The T72-3 scores exhibit a more pronounced peak near 0 degree aspect angle. At 180 degree nominal aspect, the peak correlation scores for the T72-1 images are higher than the peak scores for the T72-3 images. Conversely, at 270 degree nominal aspect, the T72-1 peak correlation scores are lower than the T72-3 peak scores. Comparing peak correlation scores (at the same nominal aspect angle) removes the effect of small aspect angle differences between the reference and match images. The differences in the peak correlations scores between Figure 4-1 and 4-7 and Figures 4-2 and 4-8 can, therefore, be attributed to intrinsic, within-class variations among the T72 tanks.

Figures 4-9 through 4-12 show T72-2 correlation scores for two confusion targets: a M60 U.S. tank (M60-3) and a T62 Soviet tank (T62-4). Comparison of the results in Figures 4-1 through 4-4 with those in Figures 4-9 through 4-12 indicates that, at most nominal aspect angles, the peak correlation scores for the two T72 tanks exceed those for the two confusion tank classes (for the same image type), indicating that the correlation scores are useful discriminants for separating the T72 tanks from the confusion tank classes. However, at 120 and 300 degree nominal aspects, the T72-2 TW peak correlation scores for the M60-3 tank exceed those for the T72-1 tank , indicating that perfect separation is not realized. In general, the correlation scores for the confusion targets show less tendency to have pronounced peaks at the cardinal aspect angles. The scores for the M60-3 match images near 180 degree aspect are significantly lower than the scores for any of the other tanks. The low scores for the T62-4 tank near 0 degree aspect indicate that its alignment may not have fallen with the ±5 degree tolerance resulting from the specific range of squint angles at which images were processed for inclusion in the expanded target chip database.

Figure 4-13 shows T72-2 correlation scores for the remaining TW T72 tanks (T72-1, T72-3, T72-4, and T72-5) near 90 degree nominal aspect. The four T72 tanks yield prominent correlation peaks at different aspect angles. The peak score for the T72-1 match images occurs at 89.5 degree aspect. Given that the T72-2 reference was obtained from the image at 90.5 degree squint, a 1 degree rotation must exist between T72-1 and T72-2 target chips at the same nominal aspect angle. The maximum angular offset occurs for the T72-5 images which appear to be rotated 3 degrees

from the T72-2 images. The angular offsets indicated by the correlation peaks are consistent with the estimates derived by visual examination of the imagery (see the classified addendum).

Figure 4-14 shows T72-2 TW correlation scores for the four confusion targets that yielded the highest peak correlation scores over the small aspect angle deviants near 90 degrees. In this case, the top four confusion targets included three of the four M60 tanks and the T62 tank. The peak confuser score illustrated in Figure 4-13, as determined from Figure 4-14, shows that all of the T72 tanks can be correctly separated from all of the confusion targets, at 90 degree nominal aspect by selection of a threshold greater than approximately 0.75. Figure 4-13 shows that the aspect angle difference between the reference and match images must be within approximately one degree to maintain T72/confuser separability. The relatively small difference between the peak correlation scores for the T72 tanks and the peak confusion target score, indicates that the reference image aspect angle increment must be maintained near 0.5 degrees to obtain the "best" chance of separating the T72 tanks from the confusion targets at 90 degree nominal aspect.

Figures 4-15 and 4-16 show corresponding T72-2 correlation scores for SVA images at 90 degree aspect angle. The correlation peaks for the T72 targets occur at approximately the same aspect angle offsets in the SVA and the TW data. The peak confuser score shown in these figures is specific to the SVA images. Figures 4-13 and 4-15 show that the difference between the peak confuser score and the lowest of the four T72 peak scores is greater for the SVA imagery than it is for the TW imagery indicating an improvement in separability using SVA at this aspect.

Figure 4-17 shows a histogram of the peak T72-2 TW correlation scores for all of the target images (four T72 tanks, four M60 tanks, one T62 tank, one 2S1 self-propelled gun, two BMP APCs, one M113 APC, and one M35 truck) at 90 degree nominal aspect. Figure 4-18 shows the comparable peak correlation scores for the SVA images. For the TW imagery, the gap between the lowest T72 score and the highest confusion target score was 0.03. For the SVA imagery, the gap increased to 0.05, indicating a slight improvement in T72/confuser separability for the SVA imagery.

Figures 4-13 and 4-15 show that the peak correlation scores for the four T72 tanks fall considerably short of the noise-limited ceilings (0.93 for TW imagery and 0.88 for SVA imagery) observed during the first phase study. Given that the T72 tanks are in similar backgrounds, the shortfall in the correlation scores must be the result of intrinsic target variability relative to the T72-2 tank. Figure 4-13 shows that the T72-2 TW correlation scores for the other T72 tanks at 90 degree aspect angle are strongly influenced by small aspect angle differences between the reference and match images and by intrinsic target variability. From a target classification standpoint,

sensitivity to small aspect angle differences can be accommodated by using more target references at small aspect angle increments. Sensitivity to intrinsic target variability represents the inherent bound on classification performance using a correlation-based algorithm.

Figures 4-19 through 4-36 show results comparable to those in Figures 4-13 through 4-18, for three additional aspect angles: 270 degrees (Figures 4-19 through 4-24), 0 degrees (Figures 4-25 through 4-30), and 120 degrees (Figures 4-31 through 4-36). At 270 degree aspect, the correlation scores for the T72 match images exhibit prominent peaks, as observed for the 90 degree aspect angle imagery. The gap between the lowest T72 score and the highest confusion target score increased from 0.07 for the TW imagery to 0.15 for the SVA imagery, providing evidence for a more significant improvement in classification performance using the SVA imagery.

At 0 degree aspect, the correlation scores for the T72 match images exhibit less tendency for prominent correlation peaks. The correlation scores for the T72 targets are very high at this aspect angles at which the signatures are dominated by a compact, high return area. The TW T72-1 match images yield high correlation scores over the entire range of aspect angles with a slight tendency to peak near -1 degree. The other T72 targets show more distinct but extended correlation peaks. For the SVA imagery, the M35 truck yields the peak confusion target score. The head-on truck signature has a dominant return area which causes its correlation score to be fairly high. The effect of this dominant return is accentuated in the SVA imagery. At 0 degree aspect angle, perfect separability is achieved between the T72 tanks and the confusion targets using either TW or SVA imagery. The difference between the minimum peak T72 score and the peak confusion target score is slightly greater in the SVA imagery (an increase from 0.07 to 0.08)

At the non-cardinal, 120 degree aspect , the scores for the T72 match images show a weak tendency for peaks in both image data types. At this aspect angle, the peak correlation scores for the T72 tanks overlap slightly onto the peak scores for the confusion targets, indicating that perfect T72/confuser separability is not attainable for either data type.

Figure 4-37 summarizes the peak T72-2 TW correlation scores at each of the twelve nominal aspect angles for the four remaining T72 tanks and the ten confusion targets. Multiple targets with the same correlation score result in a single symbol in this plot. Figure 4-38 shows the corresponding peak T72-2 SVA correlation scores. These figures illustrate that the separation between the T72 tanks and the confusion targets is very good at most aspect angles. For the TW target chips, the T72 tanks are completely separated from the confusion targets at 6 of the 12 aspect angles (0, 30,

60, 90, 150, and 270 degrees). For the SVA target chips, perfect separation is attained at 8 of the 12 angles (0, 60, 90, 150, 180, 210, 270, and 330 degrees).

Figures 4-39 through 4-42 provide corresponding graphical summaries of the peak correlation scores for the T72-3 and the M60-3 reference images. The peak T72 tank scores for the T72-3 reference images do not vary as much as for the T72-2 references. The peak scores for the T72-3 reference are not exceptionally high at 0 degree aspect as they are for the T72-1 reference. The highest score for the T72-3 references occurs at 210 degree aspect. Separability between the T72 tanks and the confusion targets is much better for the T72-2 references at 270 degree aspect than it is for the T72-3 reference. Conversely, the T72-3 reference yields better separability at 210 degrees than is the case for the T72-2 reference. The inconsistencies between the results for the two targets is a consequence of intrinsic variability. For the M60-3 TW reference, 4 misclassifications occur at 270 degrees aspect. The SVA M60-3 reference at 90 degree aspect provides considerably enhanced separation relative to the TW reference at the same aspect. The M60-3 peak correlation scores for the other 3 M60s at 240 degree aspect are quite high due to the existence of a very strong scatterer.

Figure 4-43 summarizes the results of a procedure to quantify the impact of TW and SVA processing on classification algorithm performance. For each nominal aspect angle and image type (TW or SVA), the table lists the number of confusion target misclassifications (#MC) that occur using the peak correlation scores for the T72-2 references as a discriminant measure with a classification threshold set at the lowest score among the four T72 tanks. For those aspect angles at which zero misclassifications were obtained for both TW and SVA imagery, the table also lists the difference between the lowest T72 peak score and the highest confusion target peak score as a measure of between-class separability. Using these results, the image formation algorithm yielding the best classification performance at each aspect angle was determined as follows:

- If one or more misclassifications was obtained for either data type (TW or SVA), the one with the fewest misclassifications was selected as yielding the best performance. If an equal number of misclassifications was obtained for both data types, other than zero, neither one was selected.

- If misclassifications did not occur for either data type, the one with the greatest between-class separability was selected as yielding the best performance. If the separability was the same for the both data types, neither one was selected.

For the T72-2 reference images, Figure 4-43 shows that SVA was determined to be best for 8 of the 12 aspect angles, TW was determined to be best for 2 of the 12 angles, and neither type was selected for the remaining 2 angles. The bold, shaded cells in the table indicate the metric used in assigning the best data type for each aspect angle.

Figures 4-44 and 4-45 provide similar results for the T72-3 and M60-3 references. For the T72-3 references, SVA was determined to be best for 7 aspect angles and TW was determined as best for 4 aspect angles. For the M60-3 references, SVA was determined as best for 9 aspect angles, and TW was determined as best for 3 angles.

The "best assignment" results consistently show superiority of SVA imagery over TW imagery, in terms of target classification performance. The total misclassification counts listed in Figures 4-43 through 4-45 indicate that, on average, approximately 10 misclassifications occur over each set of 120 confusion targets, including the M60 tanks and the T62 tanks. The same figures indicate that 120 degree nominal aspect consistently yields a relatively high number of misclassifications.

The results presented above were obtained using the peak correlation scores derived over the set of 21 small aspect angle deviants for each match target (T72 tanks and confusion targets). The peak correlation scores provide classification discriminants for which the reference and match images are aligned in aspect to ± 0.25 degrees. As a point of interest, T72-2 reference correlation scores were derived using the match target chips from the 90 degree squint images only. (These results are analogous to those derived during the first phase study.) Figures 4-45 and 4-46 provide graphical summaries of the resultant correlation scores for the 12 nominal aspect angles. Comparing these results to those derived over the complete sets of aspect angle deviants (Figures 4-37 and 4-38), shows that T72/confuser target separability is not nearly as good when the correlation scores are optimized in terms of the angular alignment between the reference and match images. For the TW imagery, 35 misclassifications occur following the procedure discussed above. For the SVA imagery, 25 misclassifications occur. Applying the procedure for selecting the best data type in terms of classification performance, SVA would be best for 5 aspect angles, TW would be best for 1 angle, and no selection would be made for 6 angles.

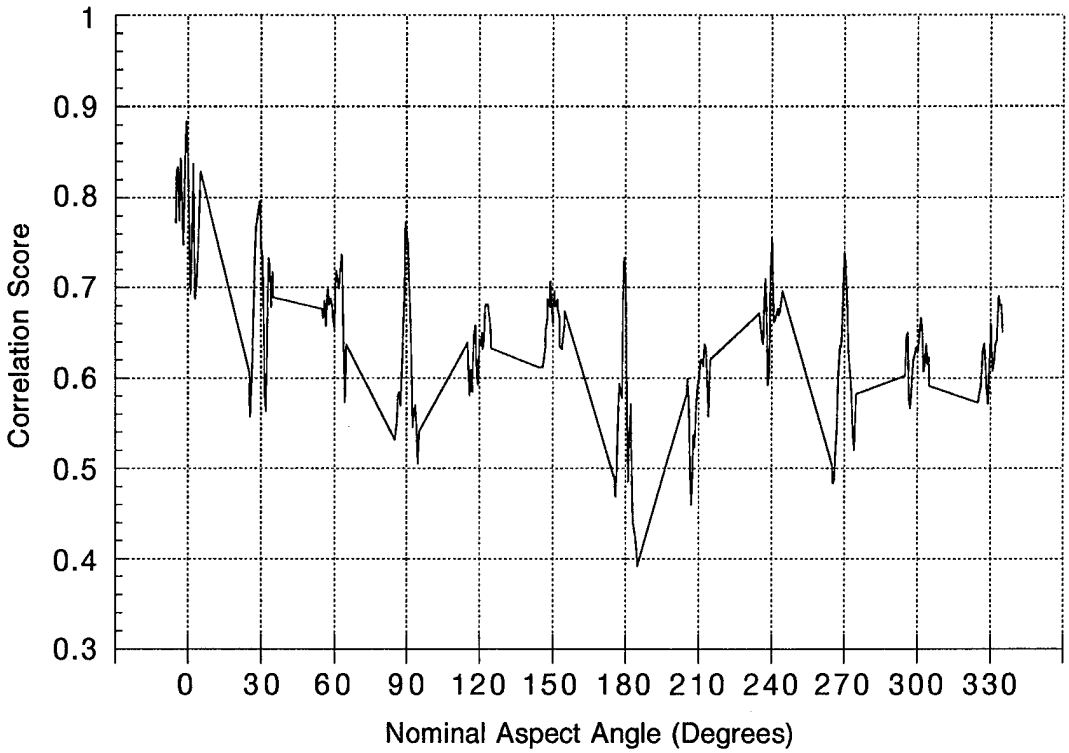

Figure 4-1. Scores for TW T72-2 Reference Correlation Against T72-1 Match Images

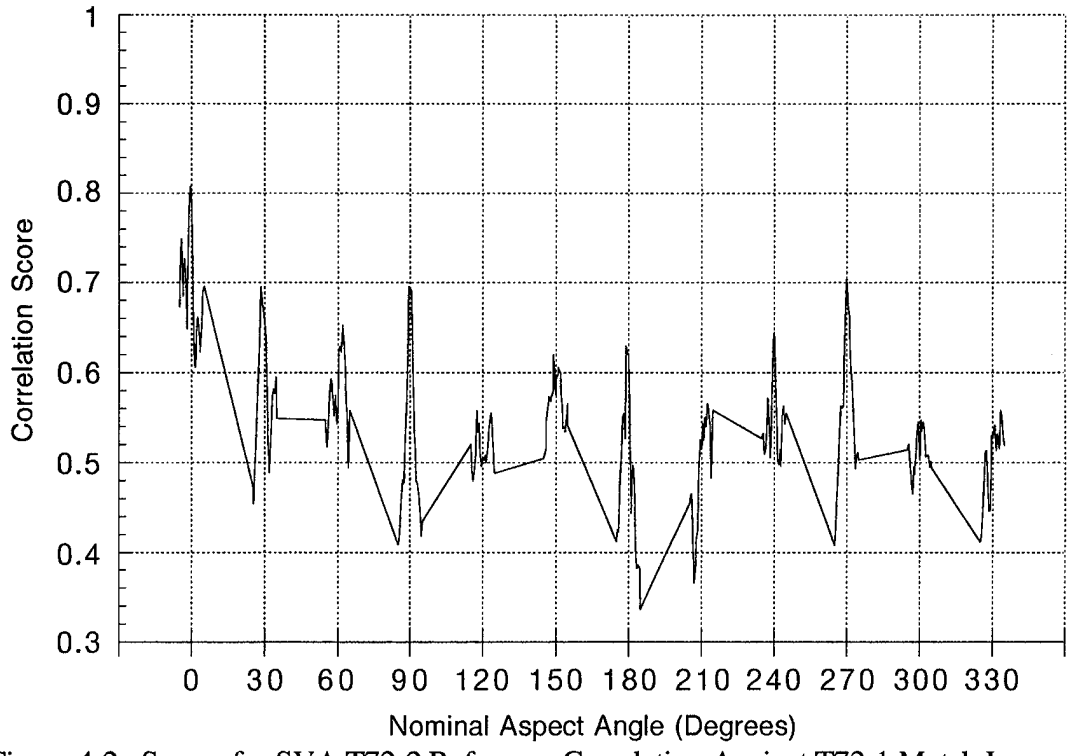

Figure 4-2. Scores for SVA T72-2 Reference Correlation Against T72-1 Match Images

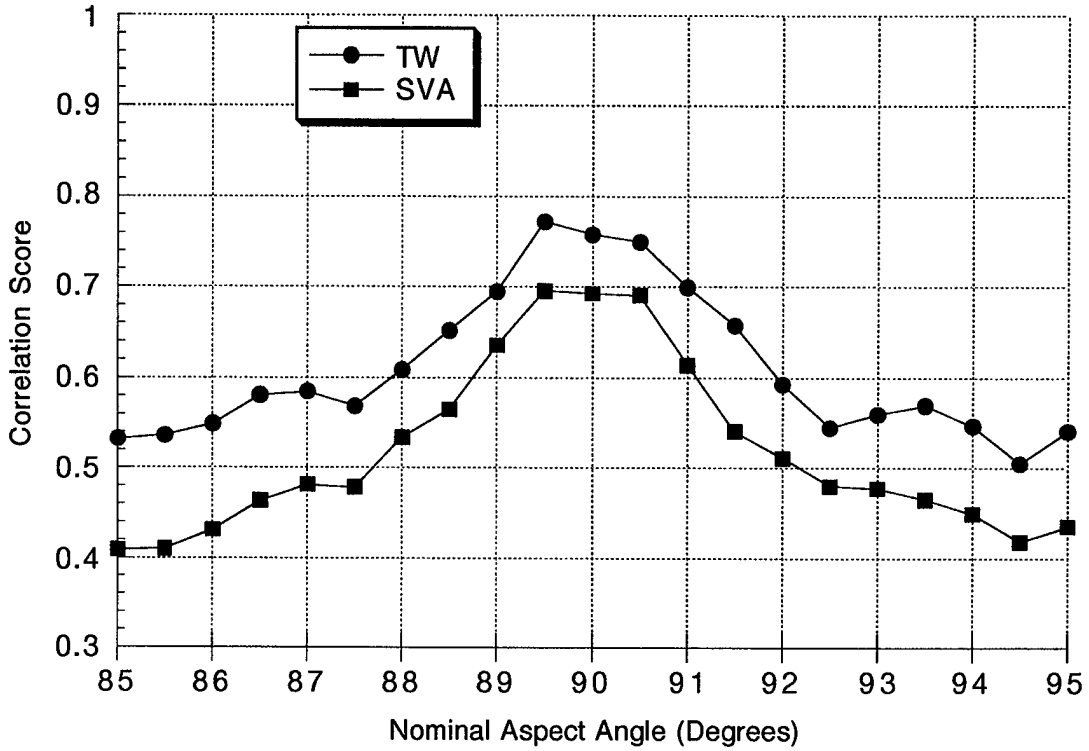

Figure 4-3 Scores for TW and SVA T72-2 Reference Correlation Against T72-1 Match Images Near 90 Degree Nominal Aspect Angle

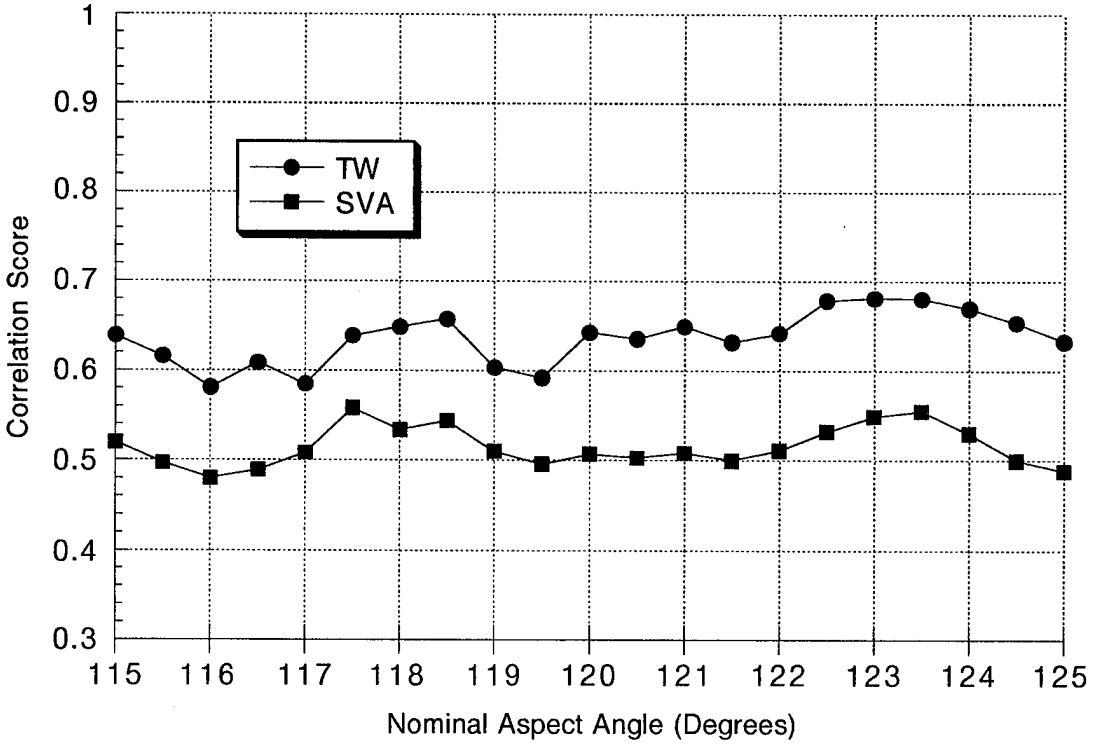

Figure 4-4. Scores for TW and SVA T72-2 Reference Correlation Against T72-1 Match Images Near 120 Degree Nominal Aspect Angle

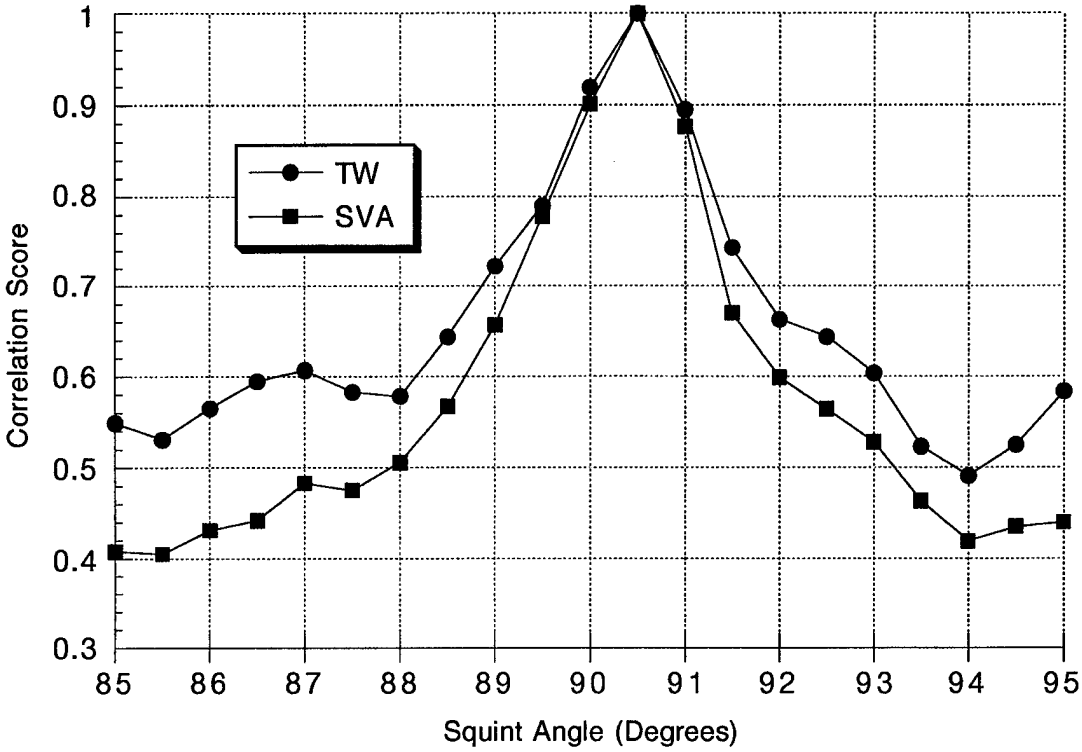

Figure 4-5. Scores for TW and SVA T72-2 Reference Correlation Against T72-2 Match Images Near 90 Degree Nominal Aspect Angle

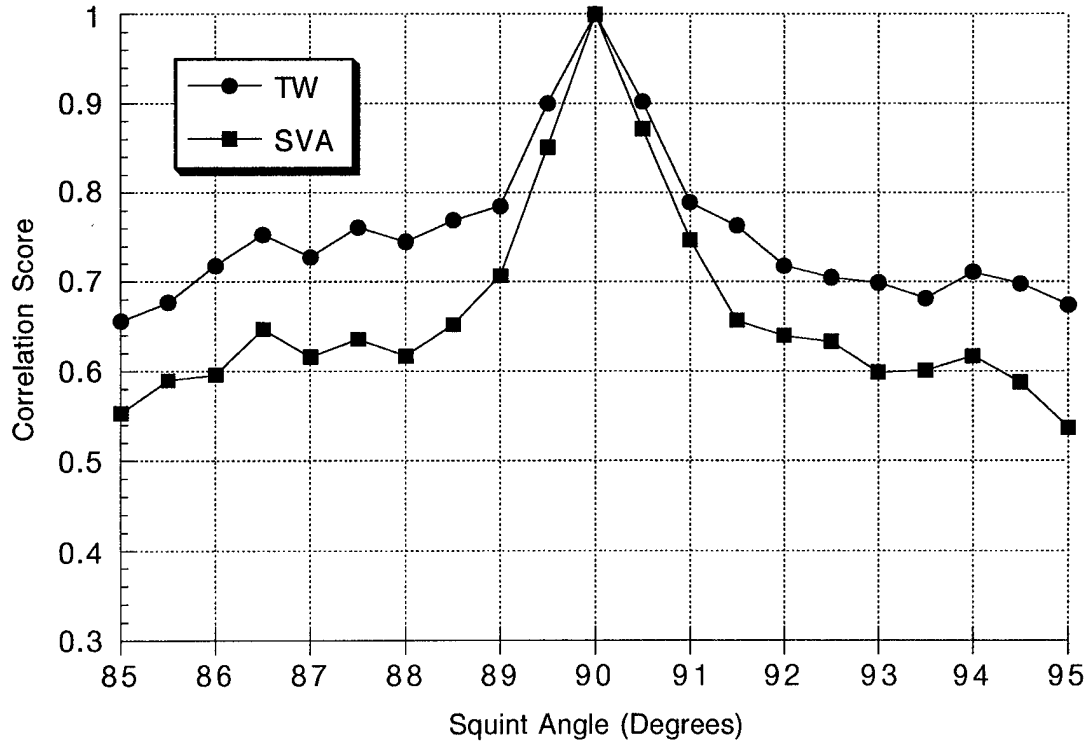

Figure 4-6. Scores for TW and SVA T72-2 Reference Correlation Against T72-2 Match Images Near 120 Degree Nominal Aspect Angle

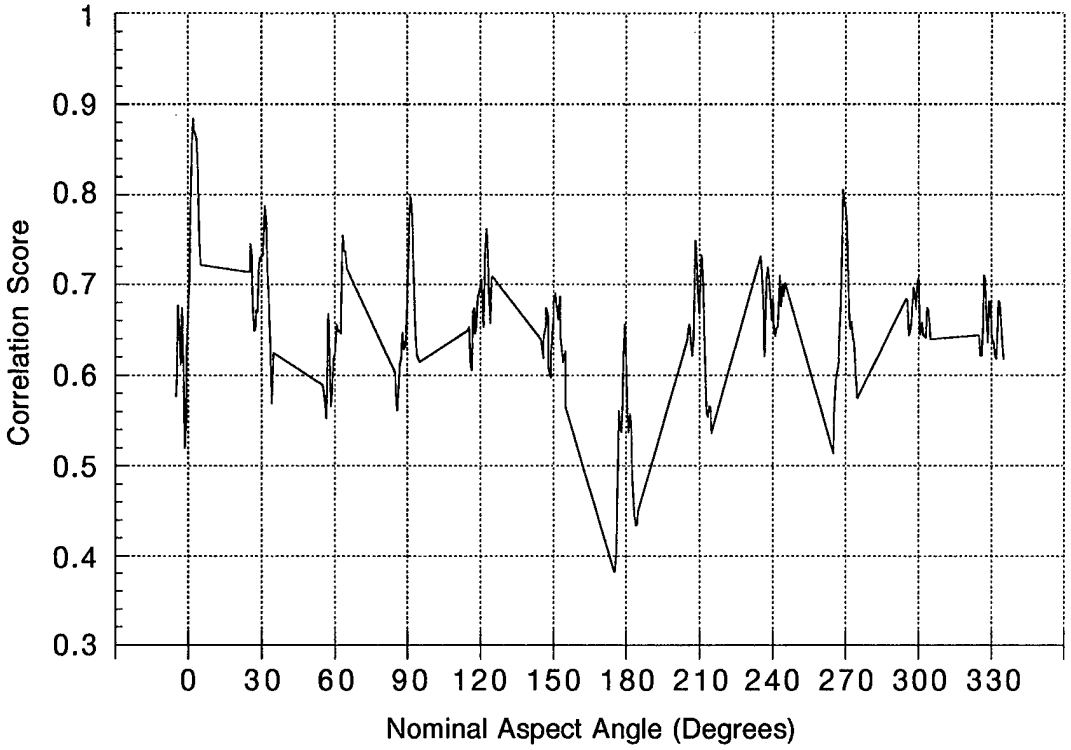

Figure 4-7. Scores for TW T72-2 Reference Correlation Against T72-3 Match Images

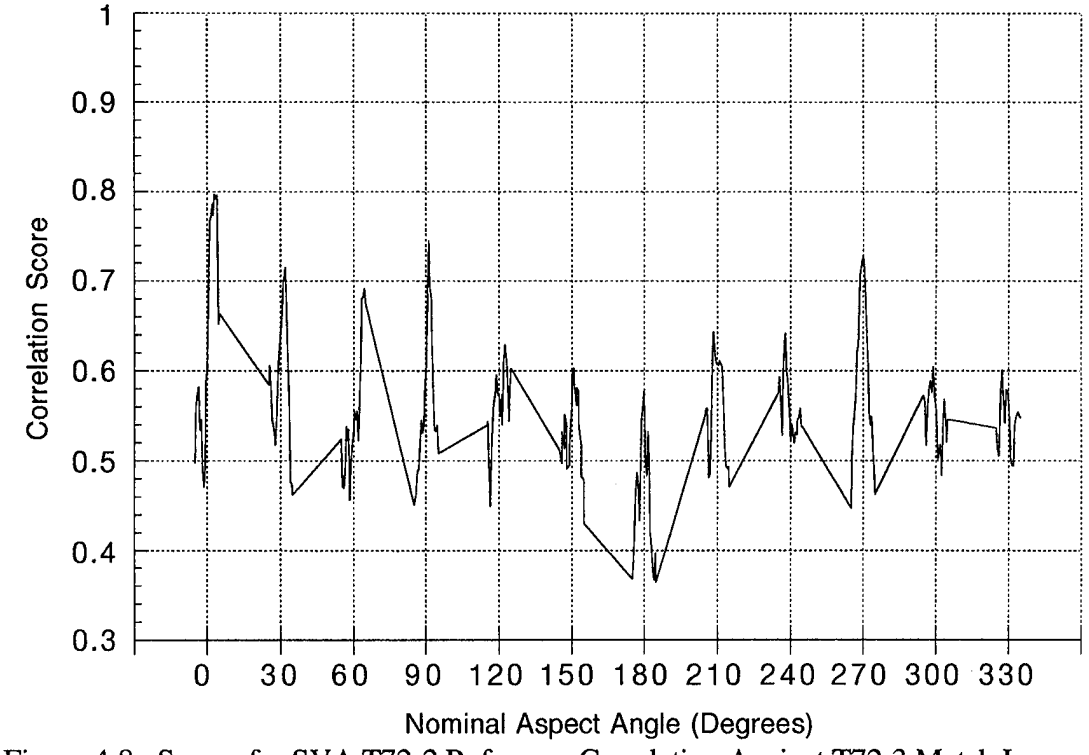

Figure 4-8. Scores for SVA T72-2 Reference Correlation Against T72-3 Match Images

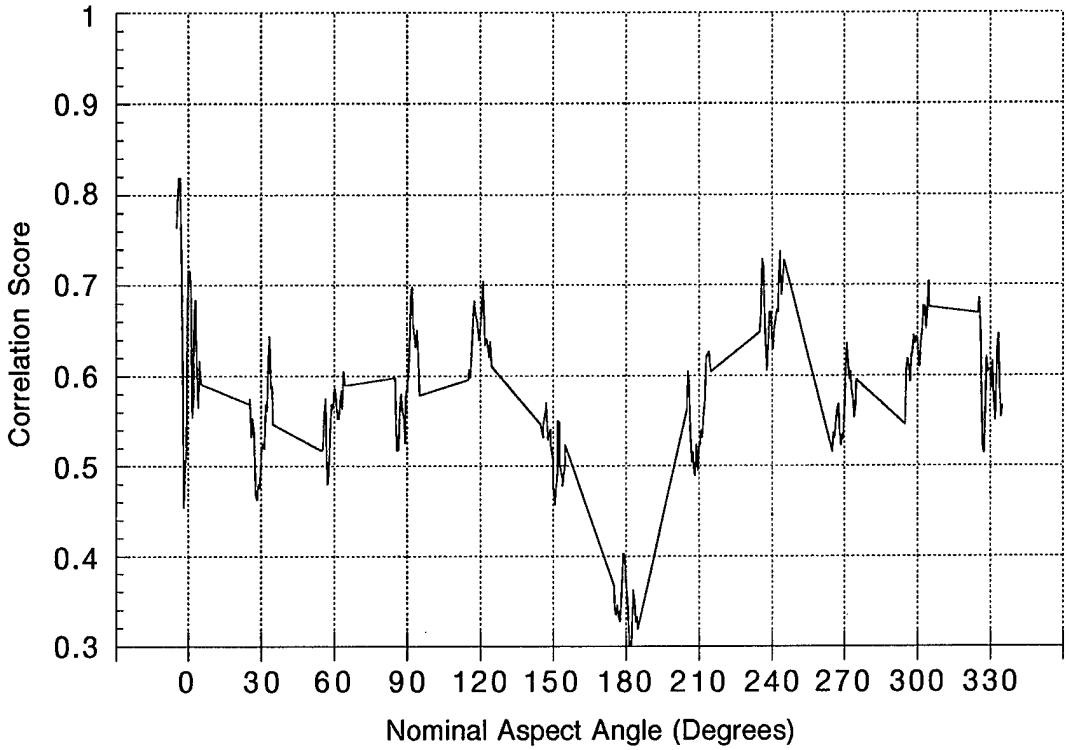

Figure 4-9. Scores for TW T72-2 Reference Correlation Against M60-3 Match Images

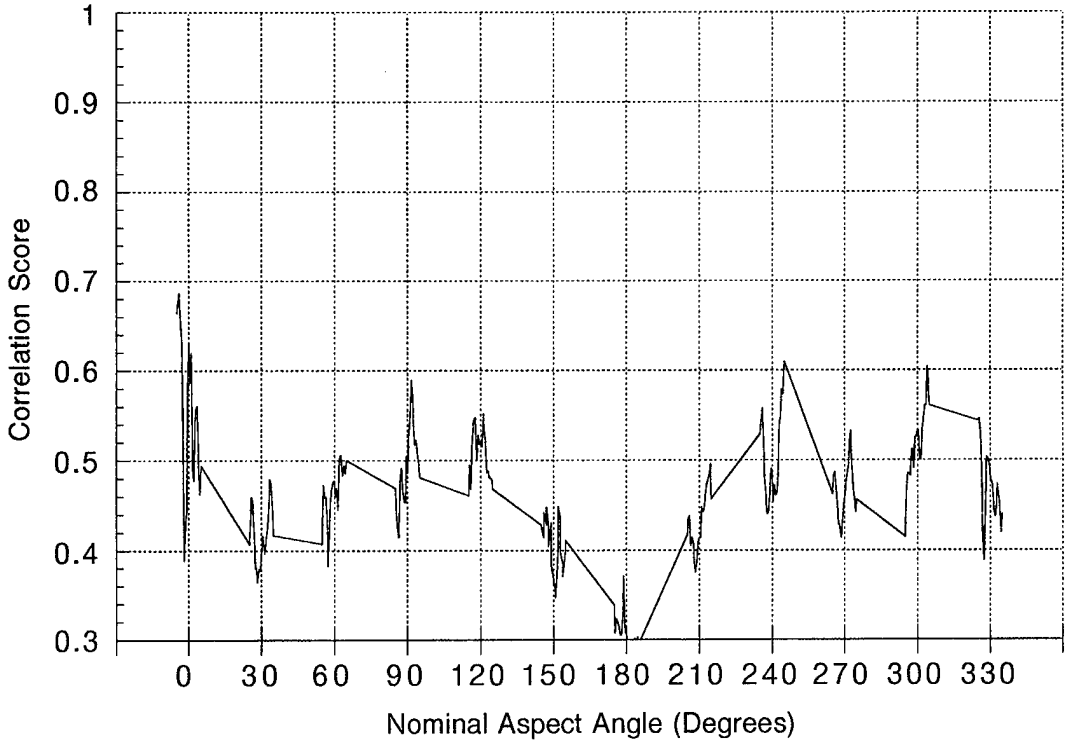

Figure 4-10. Scores for SVA T72-2 Reference Correlation Against M60-3 Match Images

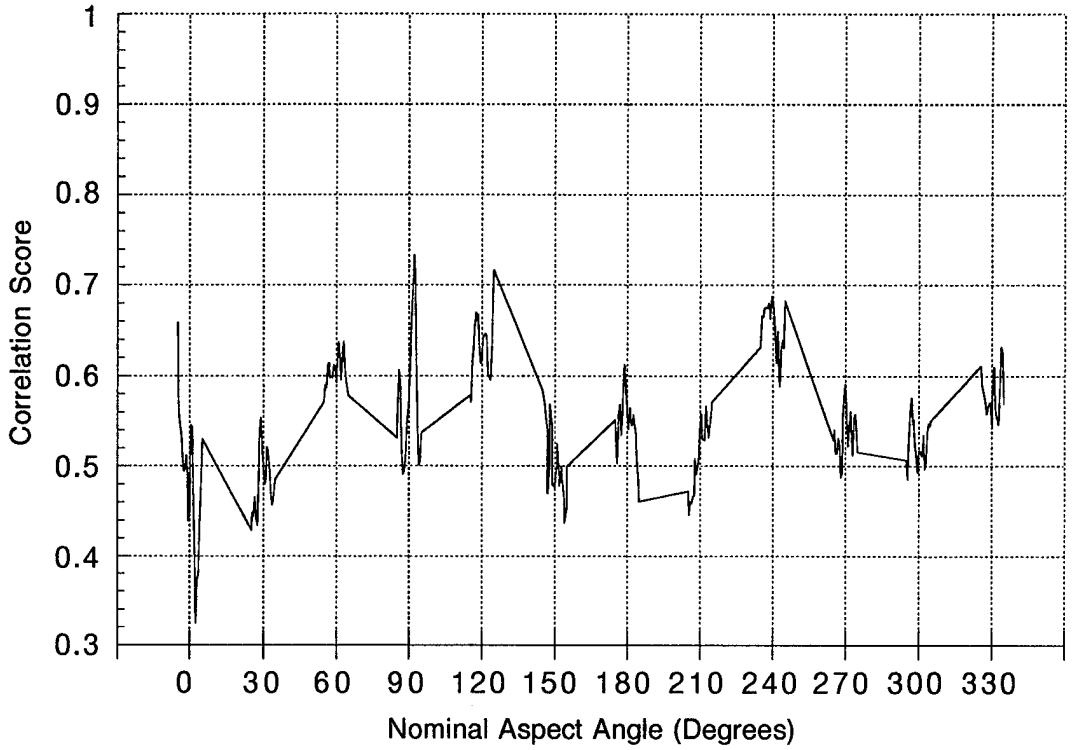

Figure 4-11. Scores for TW T72-2 Reference Correlation Against T62-4 Match Images

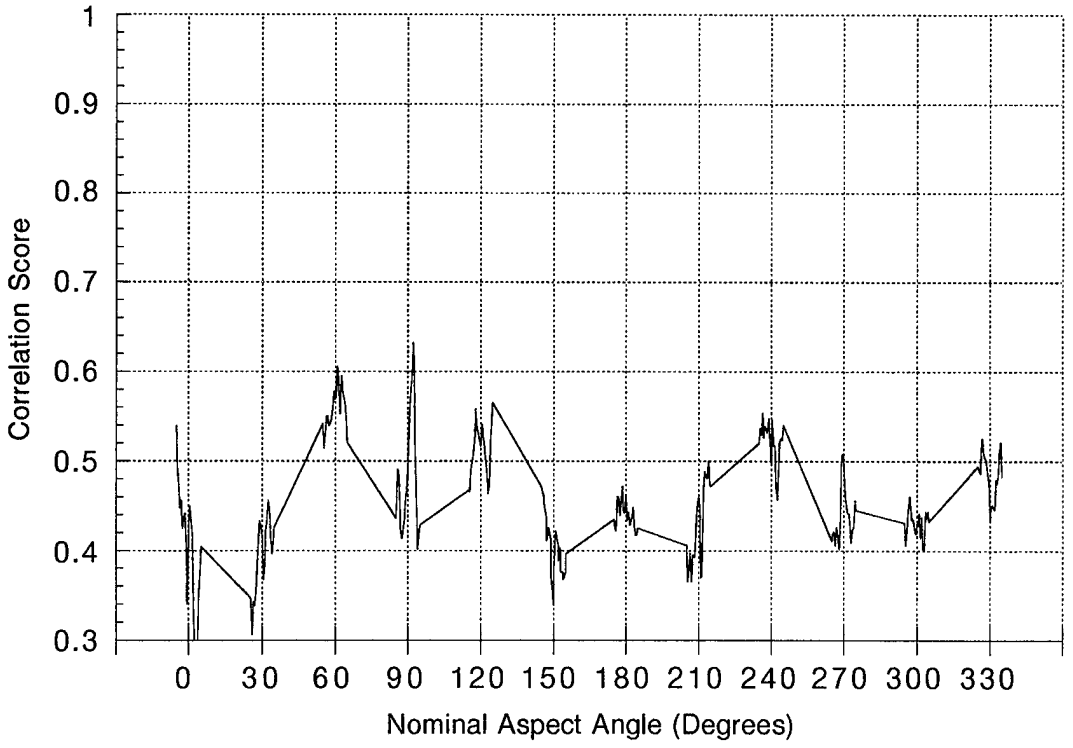

Figure 4-12. Scores for SVA T72-2 Reference Correlation Against T62-4 Match Images

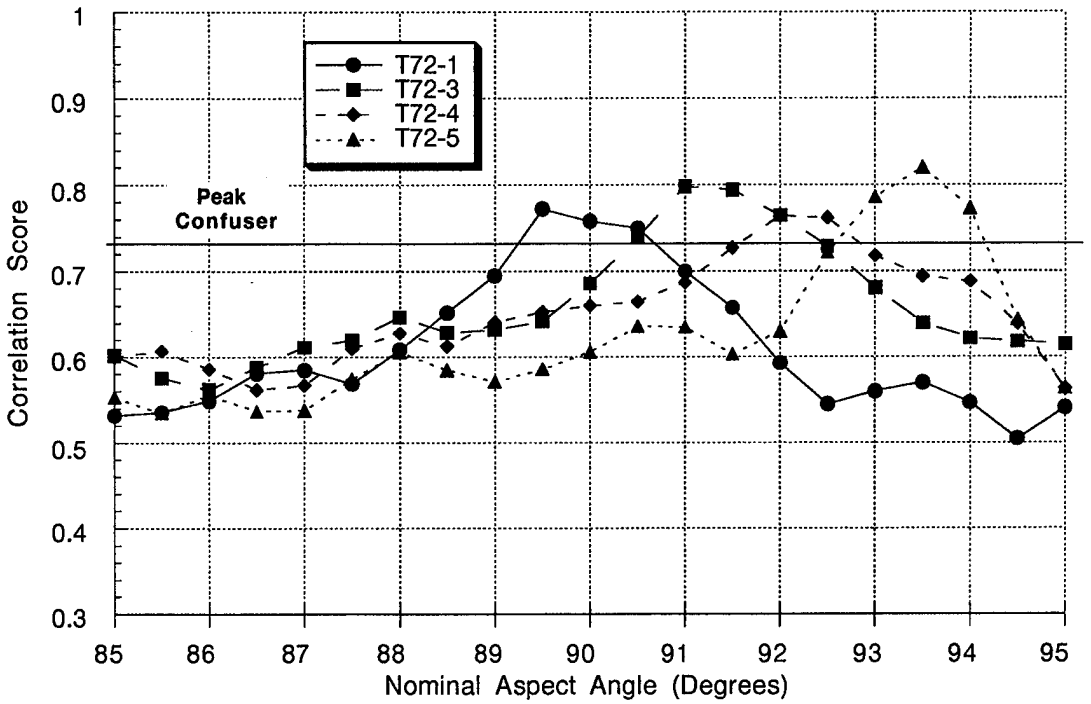

Figure 4-13. Scores for TW T72-2 Reference Correlation Against T72 Target Images at 90 Degree Nominal Aspect Angle

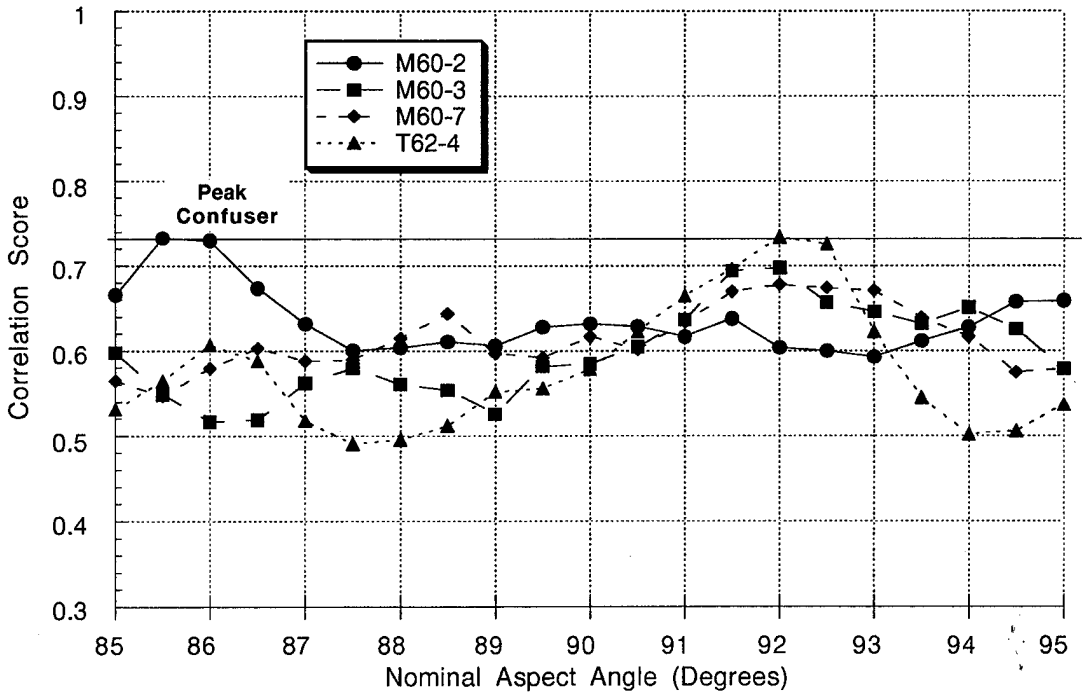

Figure 4-14. Scores for TW T72-2 Reference Correlation Against Top Four Confusion Target Images at 90 Degree Nominal Aspect Angle

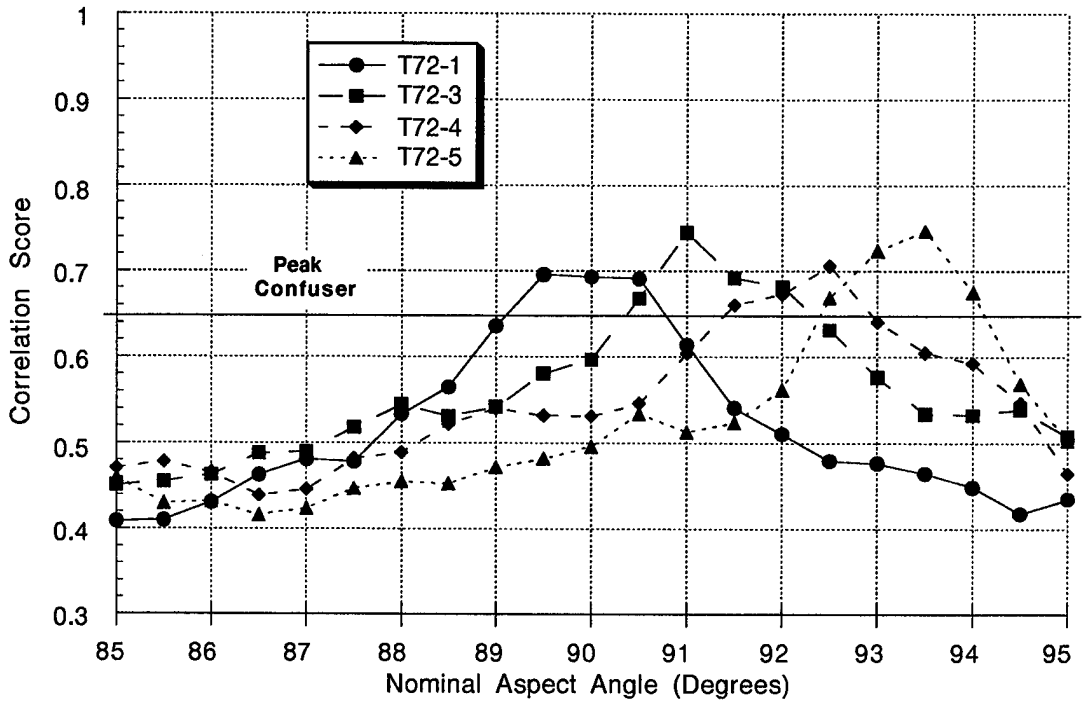

Figure 4-15. Scores for SVA T72-2 Reference Correlation Against T72 Target Images at 90 Degree Nominal Aspect Angle

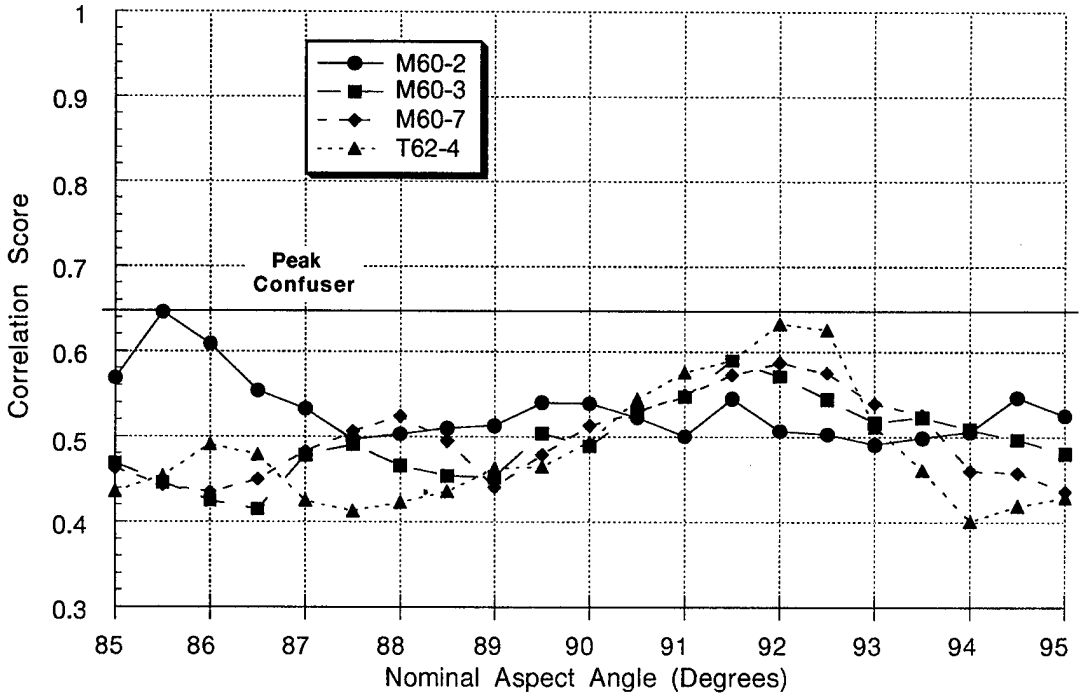

Figure 4-16. Scores for SVA T72-2 Reference Correlation Against Top Four Confusion Target Images at 90 Degree Nominal Aspect Angle

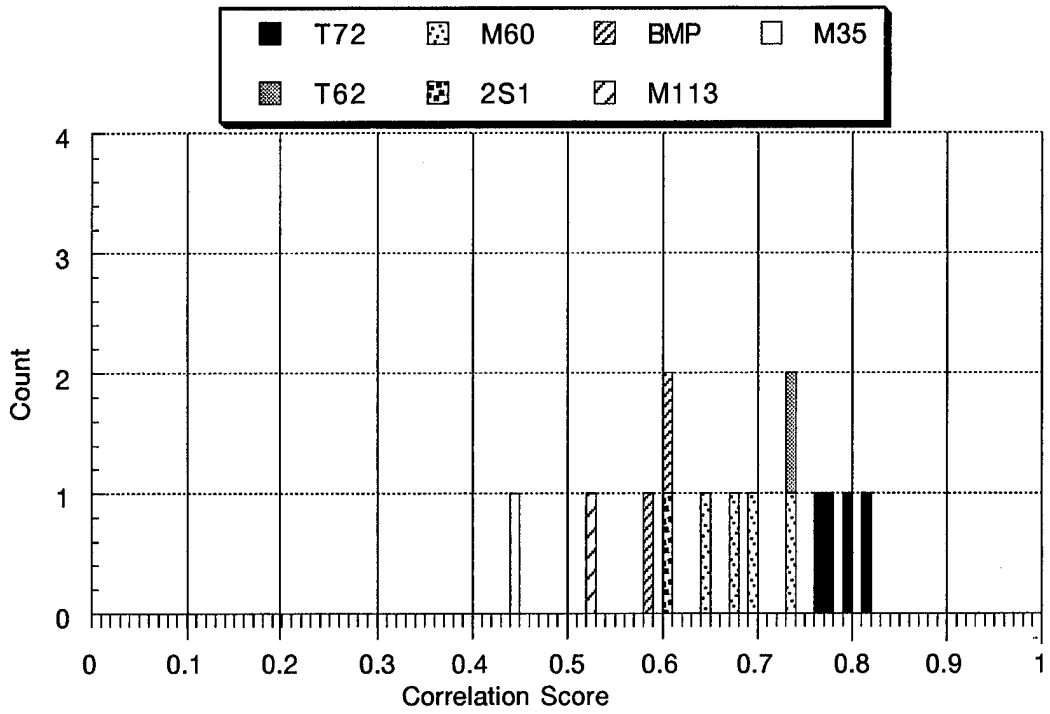

Figure 4-17. Peak Scores for T72-2 TW Reference Correlation Against All Target Images at 90 Degree Nominal Aspect Angle

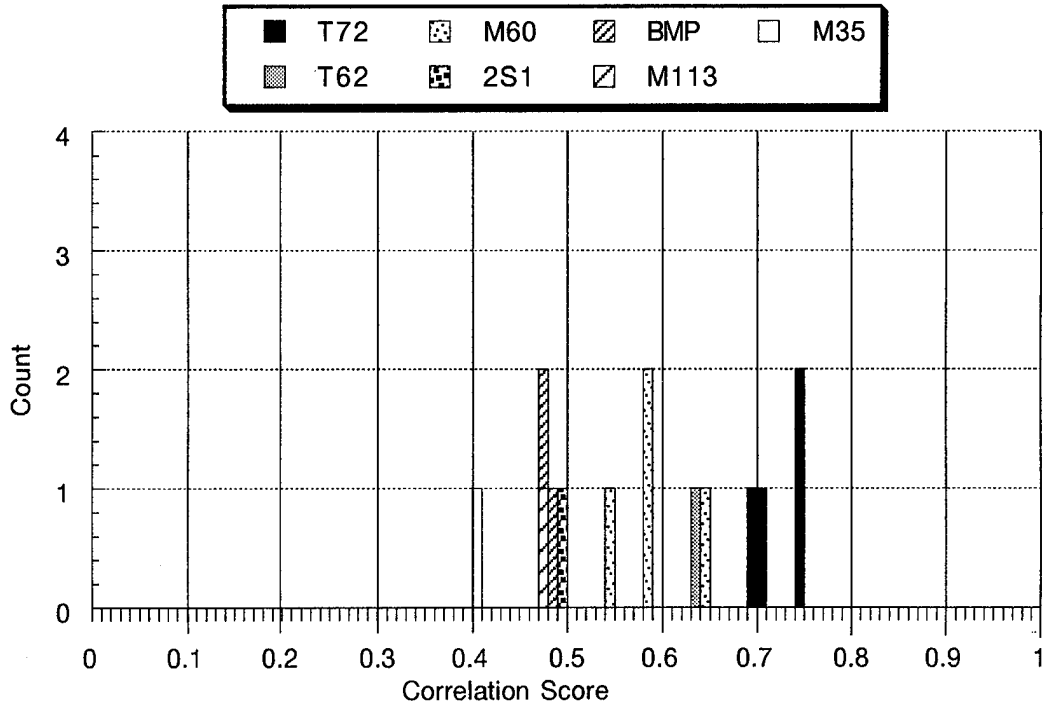

Figure 4-18. Peak Scores for T72-2 SVA Reference Correlation Against All Target Images at 90 Degree Nominal Aspect Angle

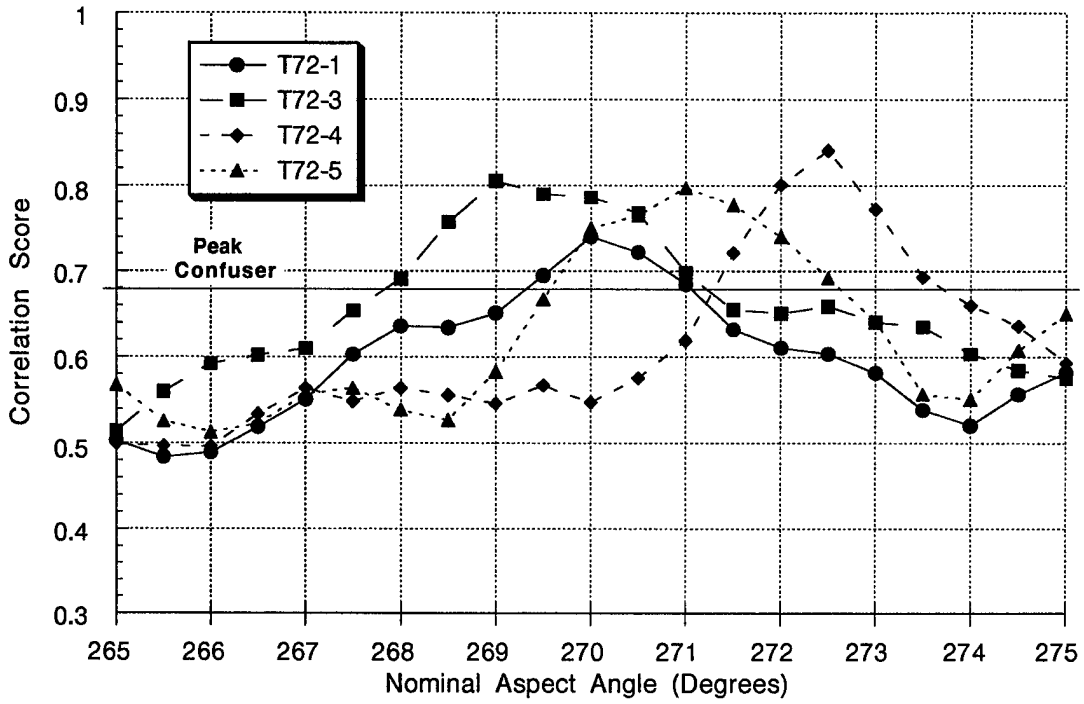

Figure 4-19. Scores for TW T72-2 Reference Correlation Against T72 Target Images at 270 Degree Nominal Aspect Angle

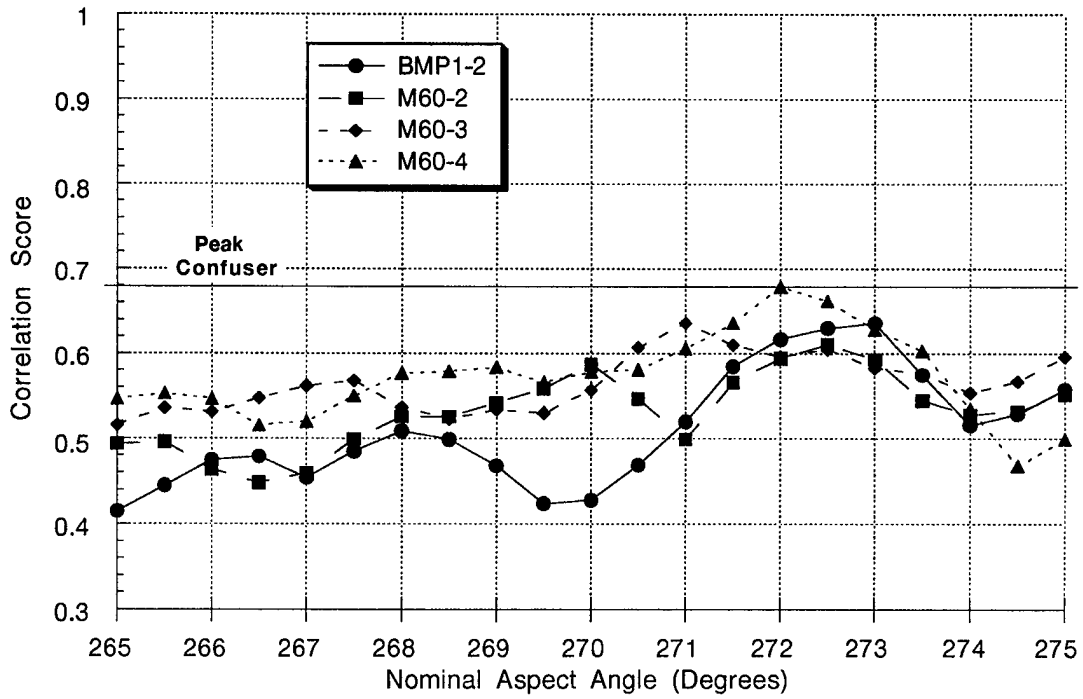

Figure 4-20. Scores for TW T72-2 Reference Correlation Against Top Four Confusion Target Images at 270 Degree Nominal Aspect Angle

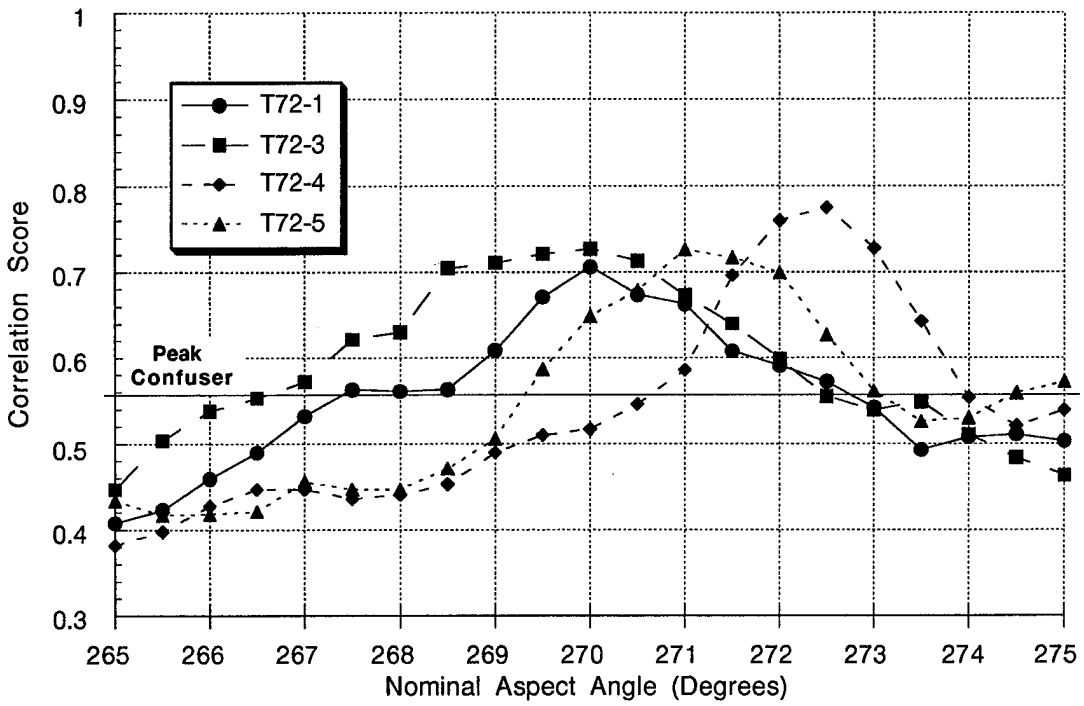

Figure 4-21. Scores for T72-2 SVA Reference Correlation Against T72 Target Images at 270 Degree Nominal Aspect Angle

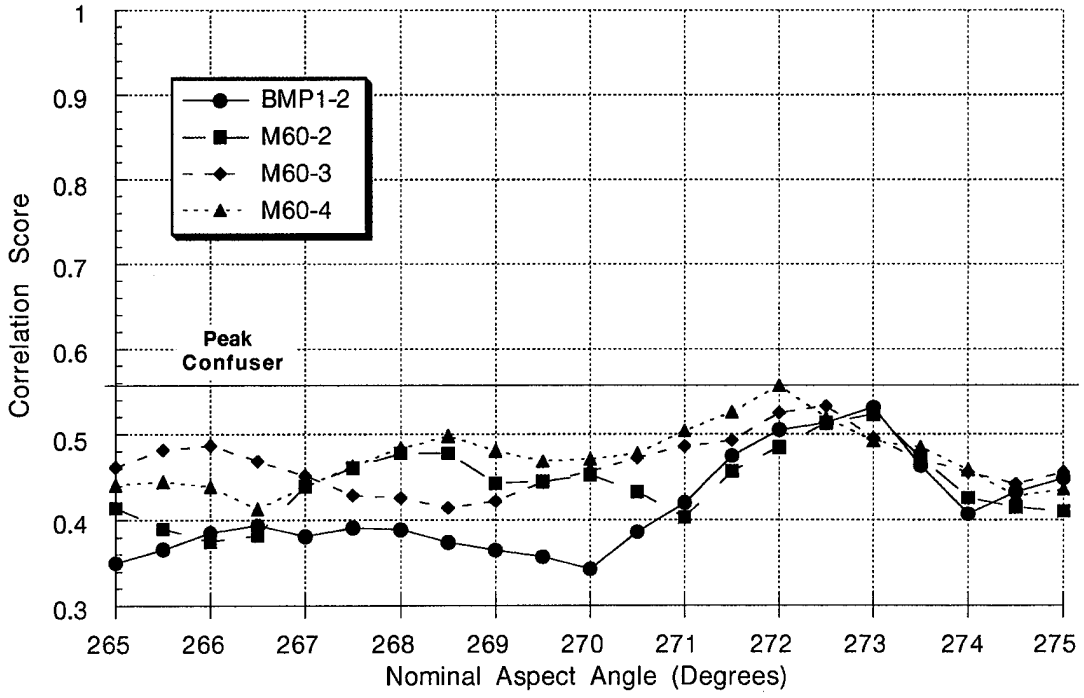

Figure 4-22. Scores for T72-2 SVA Reference Correlation Against Top Four Confusion Target Images at 270 Degree Nominal Aspect Angle

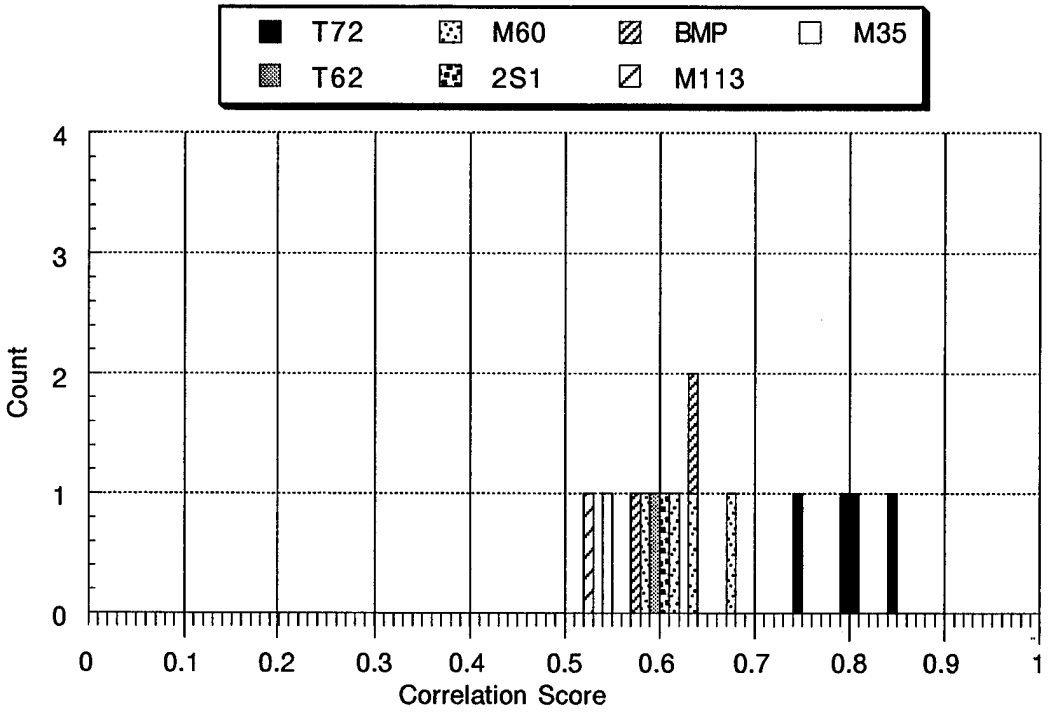

Figure 4-23. Peak Scores for TW T72-2 Reference Correlation Against All Target Images at 270 Degree Nominal Aspect Angle

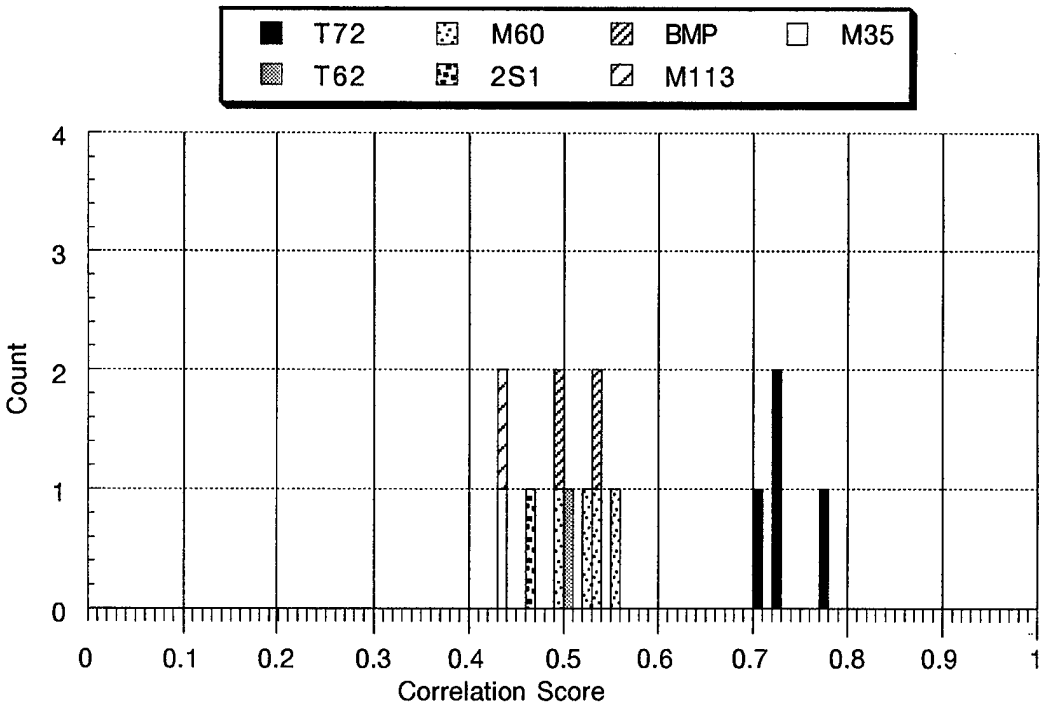

Figure 4-24. Peak Scores for SVA T72-2 Reference Correlation Against All Target Images at 270 Degree Nominal Aspect Angle

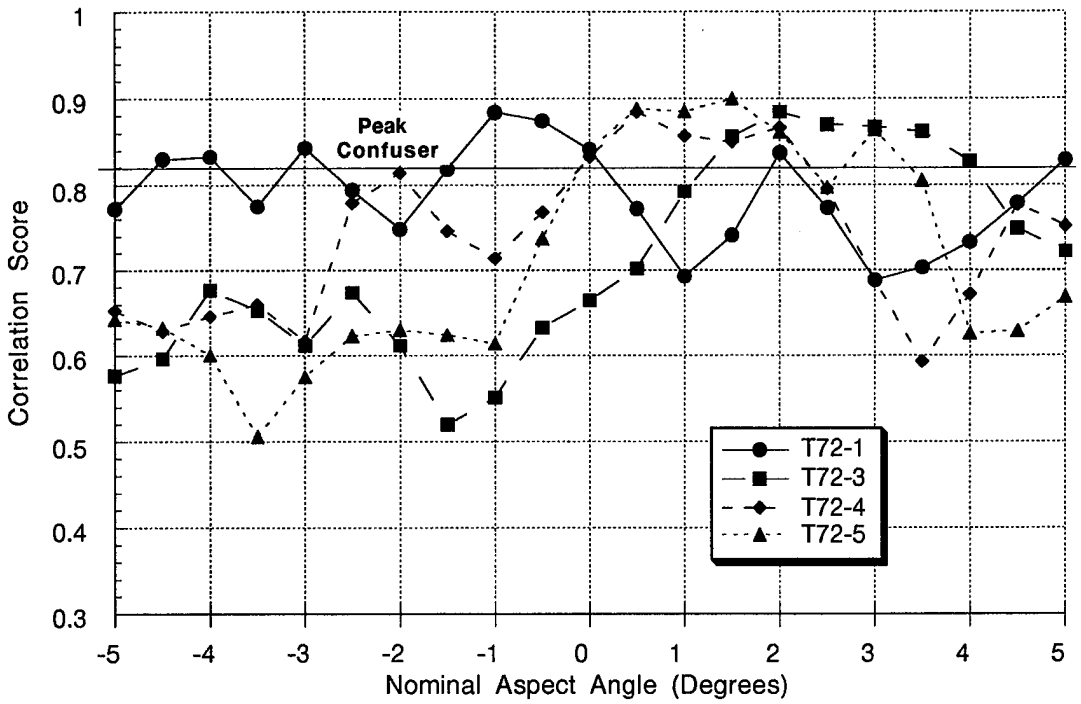

Figure 4-25. Scores for TW T72-2 Reference Correlation Against T72 Target Images at 0 Degree Nominal Aspect Angle

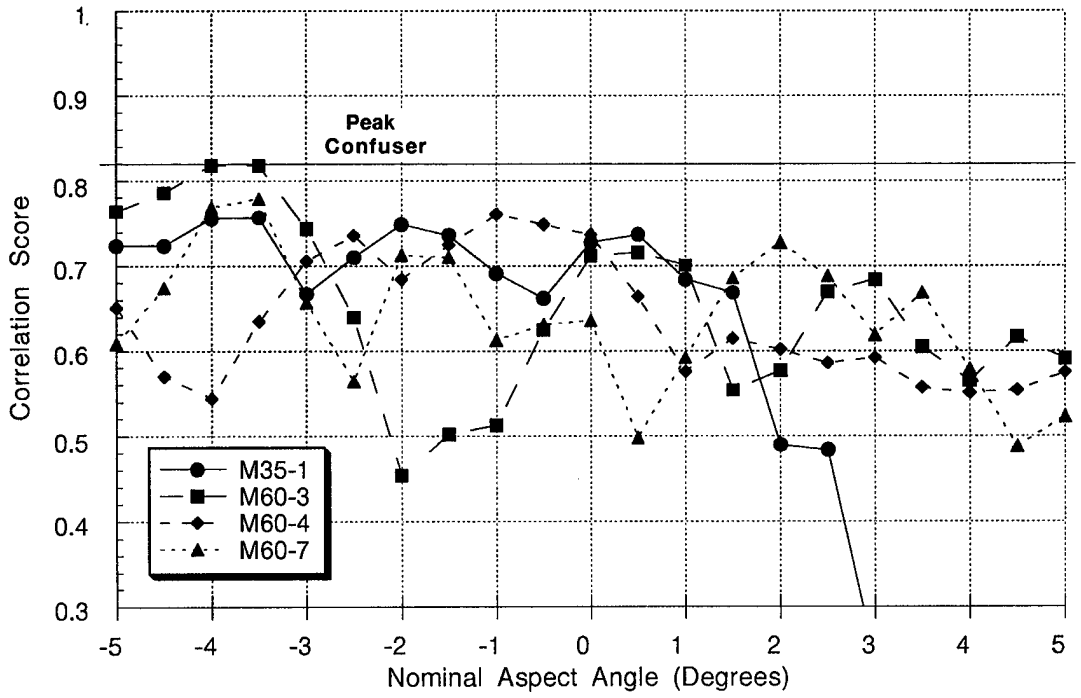

Figure 4-26. Scores for TW T72-2 Reference Correlation Against Top Four Confusion Target Images at 0 Degree Nominal Aspect Angle

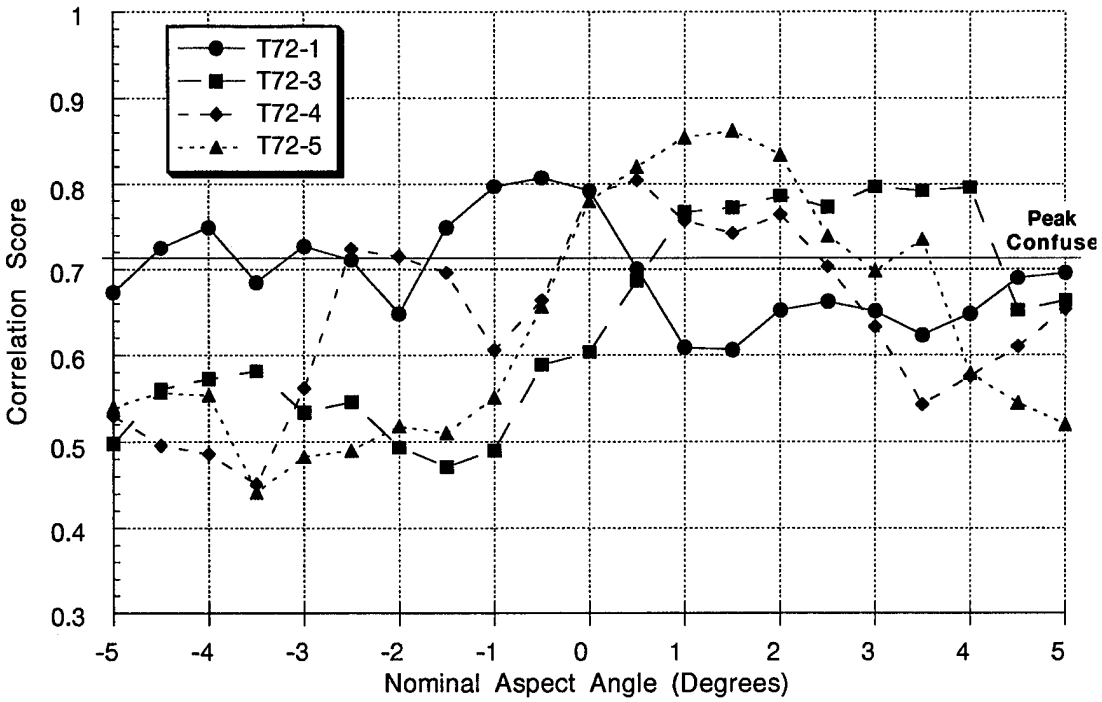

Figure 4-27. Scores for SVA T72-2 Reference Correlation Against T72 Target Images at 0 Degree Nominal Aspect Angle

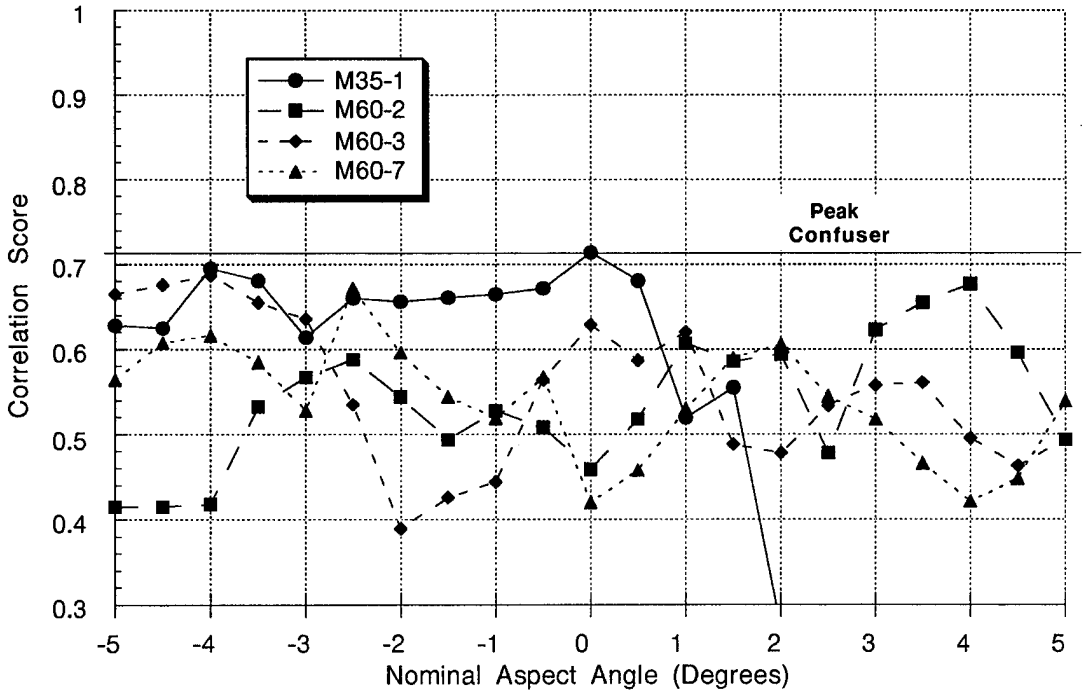

Figure 4-28. Scores for SVA T72-2 Reference Correlation Against Top Four Confusion Target Images at 0 Degree Nominal Aspect Angle

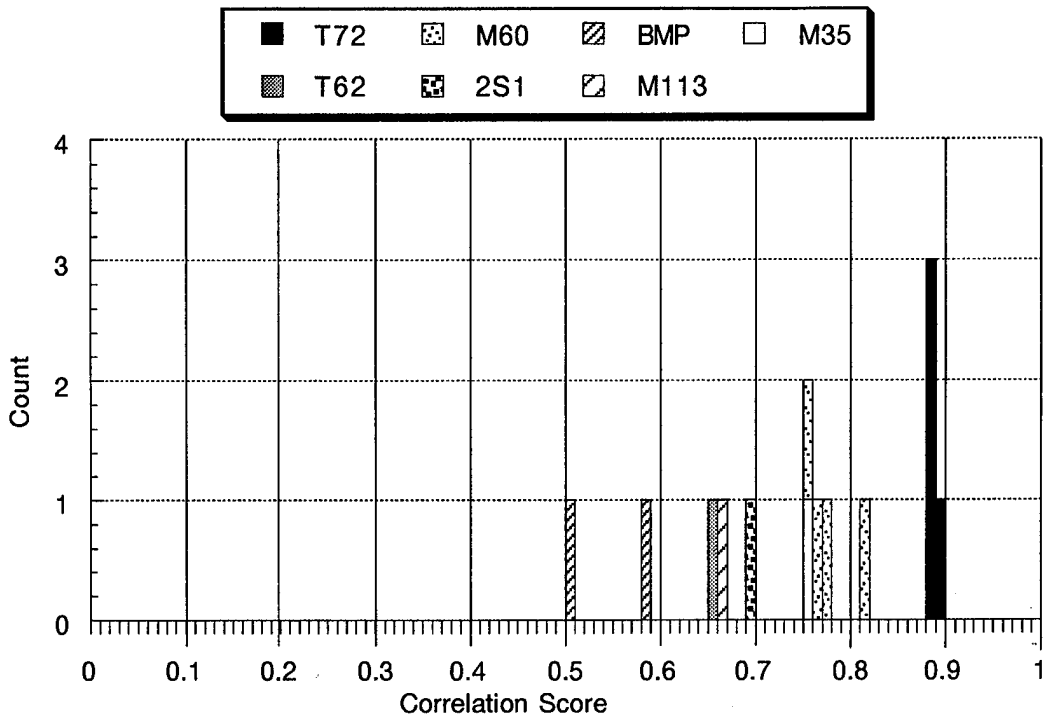

Figure 4-29. Peak Scores for T72-2 TW Reference Correlation Against All Target Images at 0 Degree Nominal Aspect Angle

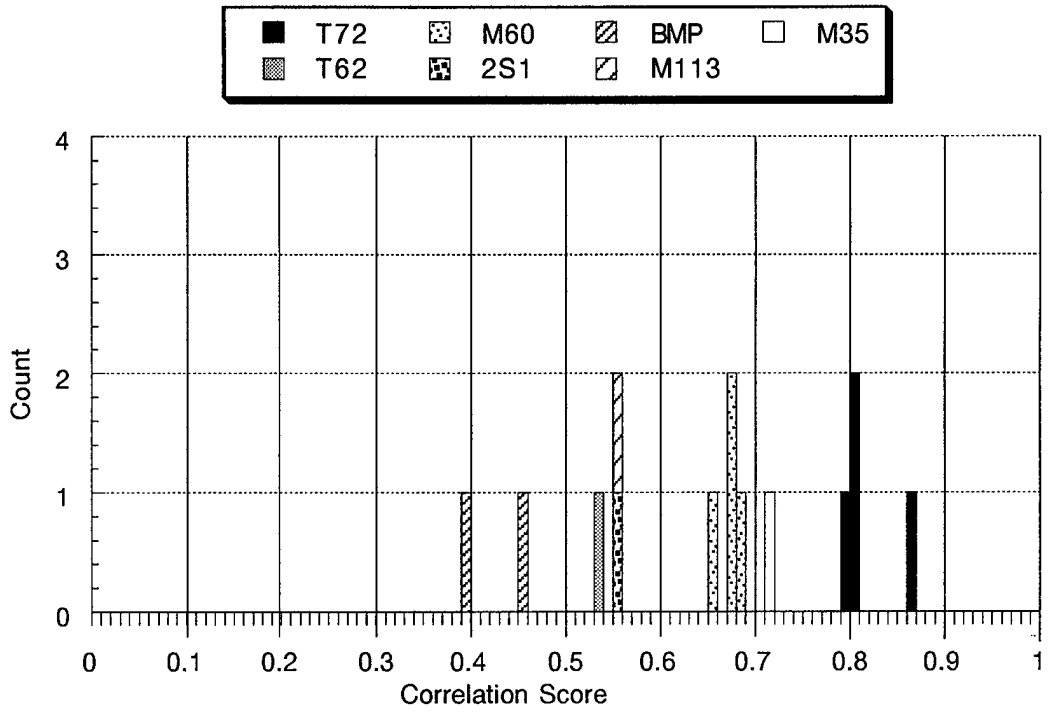

Figure 4-30. Peak Scores for T72-2 SVA Reference Correlation Against All Target Images at 0 Degree Nominal Aspect Angle

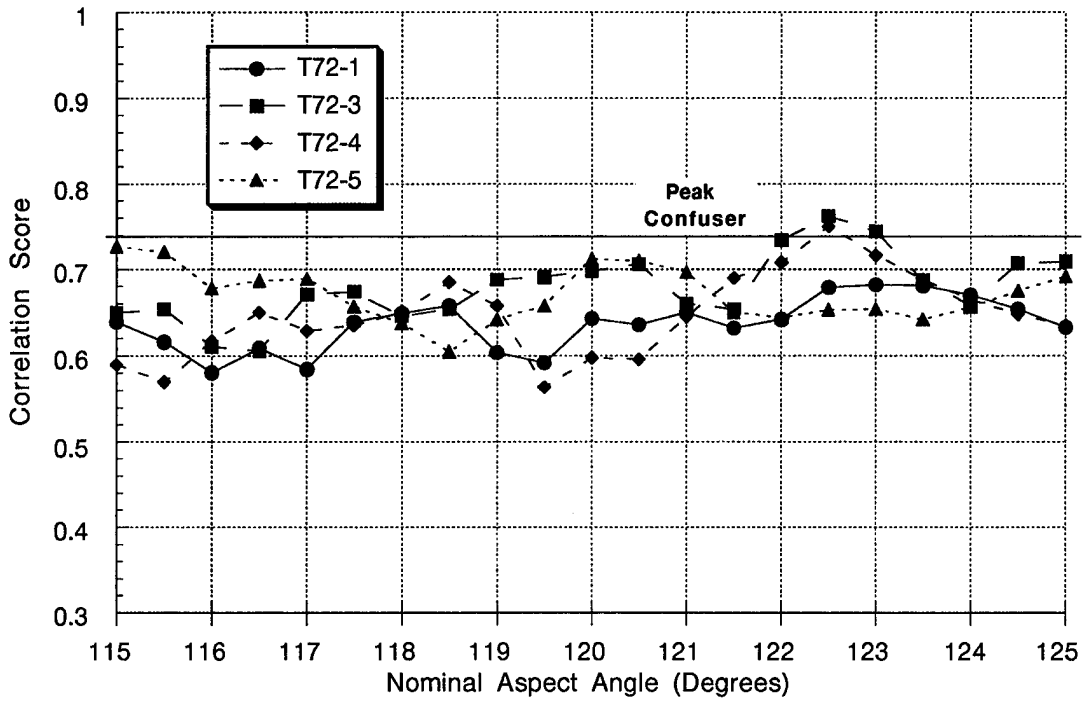

Figure 4-31. Scores for TW T72-2 Reference Correlation Against T72 Target Images at 120 Degree Nominal Aspect Angle

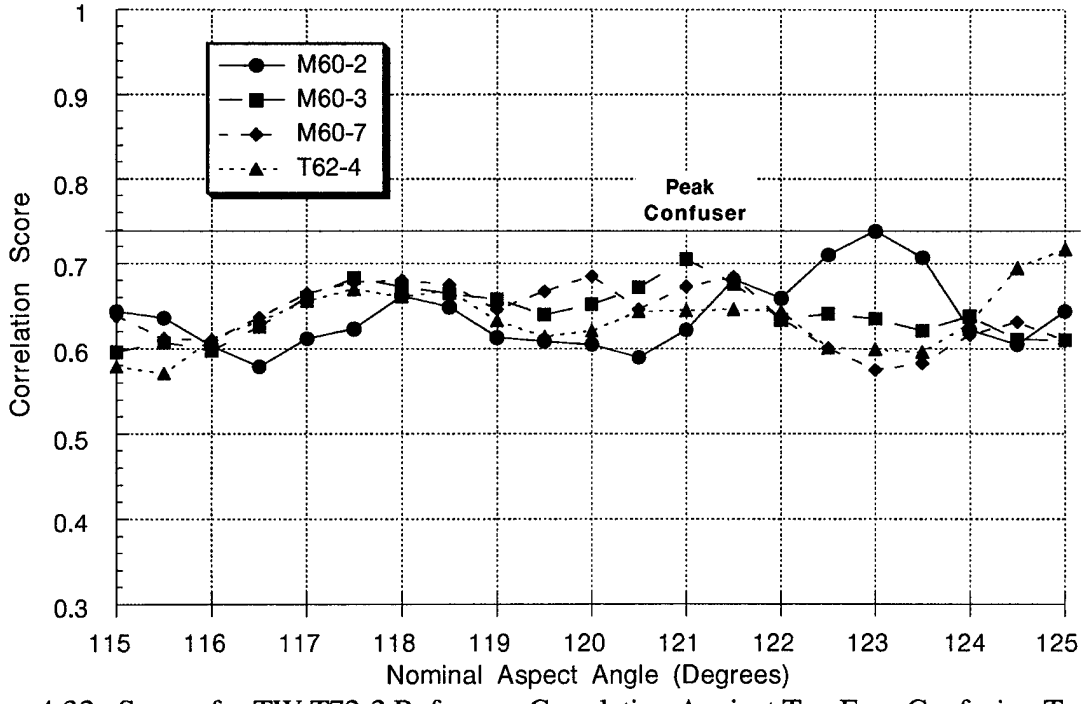

Figure 4-32. Scores for TW T72-2 Reference Correlation Against Top Four Confusion Target Images at 120 Degree Nominal Aspect Angle

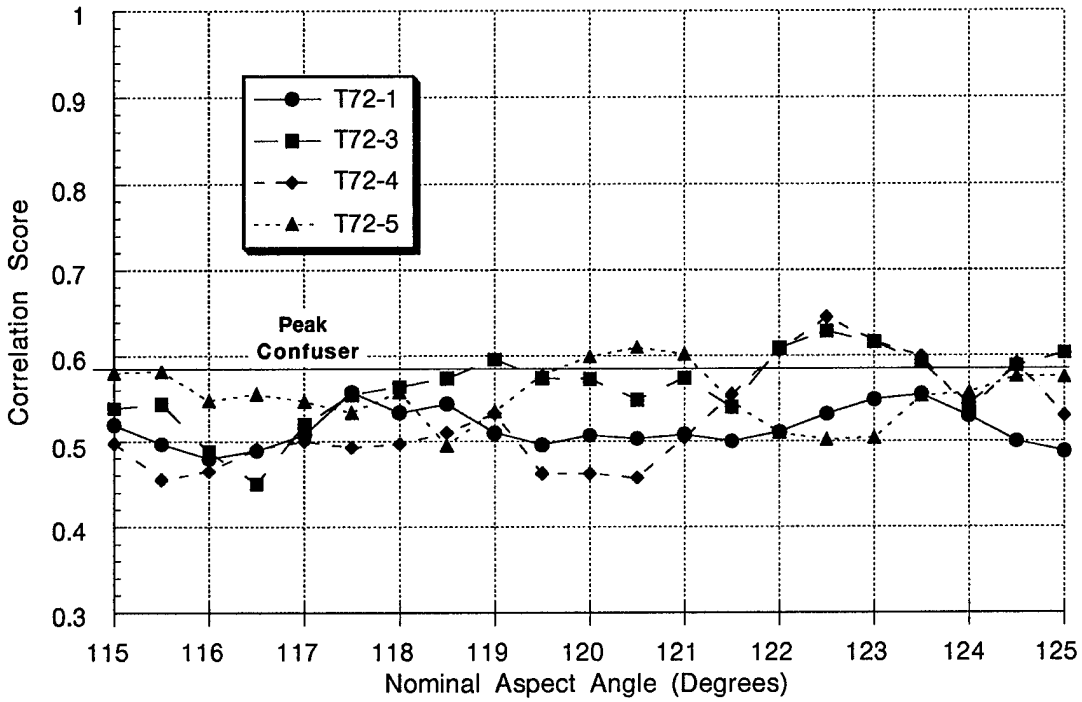

Figure 4-33. Scores for SVA T72-2 Reference Correlation Against T72 Target Images at 120 Degree Nominal Aspect Angle

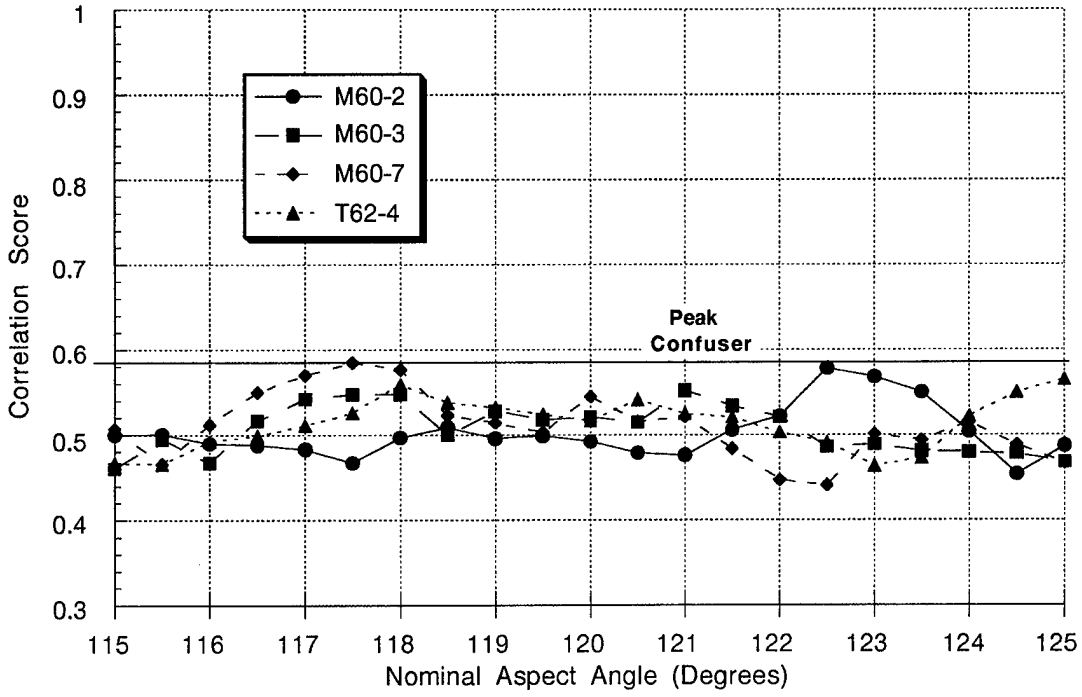

Figure 4-34. Scores for SVA T72-2 Reference Correlation Against Top Four Confusion Target Images at 120 Degree Nominal Aspect Angle

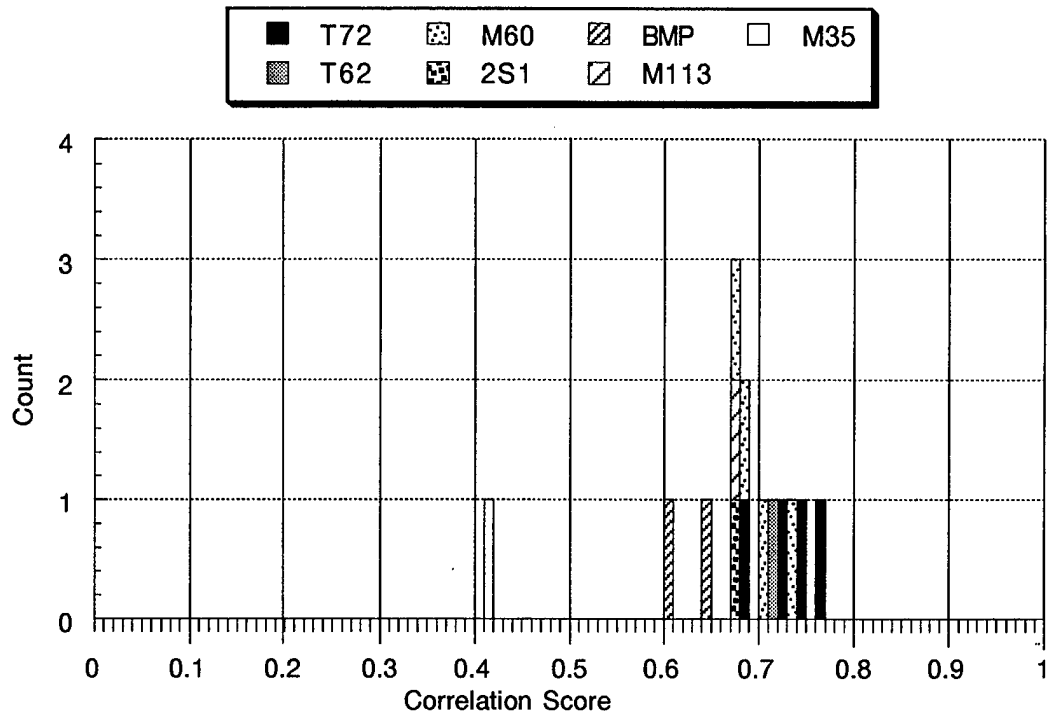

Figure 4-35. Peak Scores for T72-2 TW Reference Correlation Against All Target Images at 120 Degree Nominal Aspect Angle

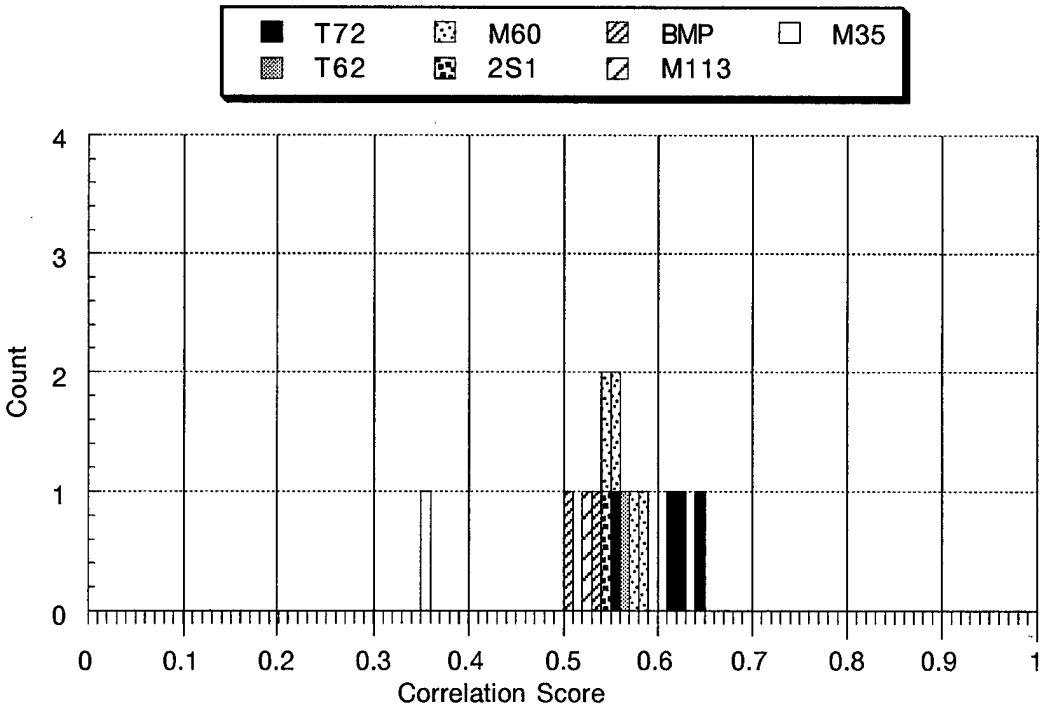

Figure 4-36. Peak Scores for T72-2 SVA Reference Correlation Against All Target Images at 120 Degree Nominal Aspect Angle

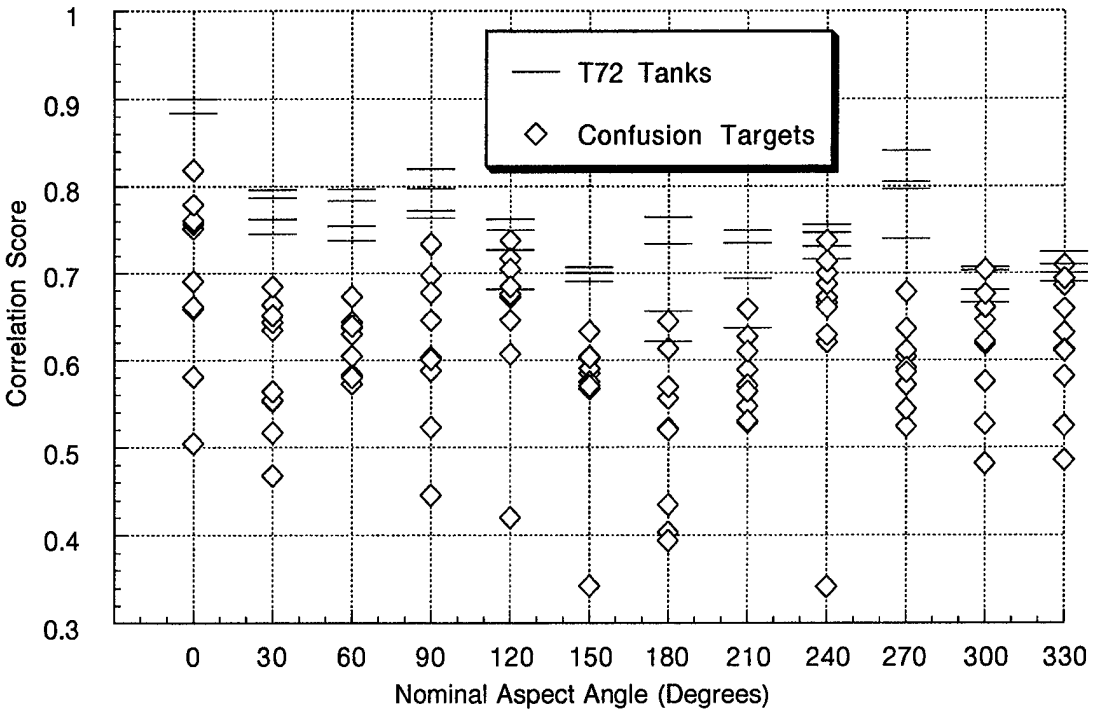

Figure 4-37. Peak Scores for T72-2 TW Reference Correlation Against All Target Images

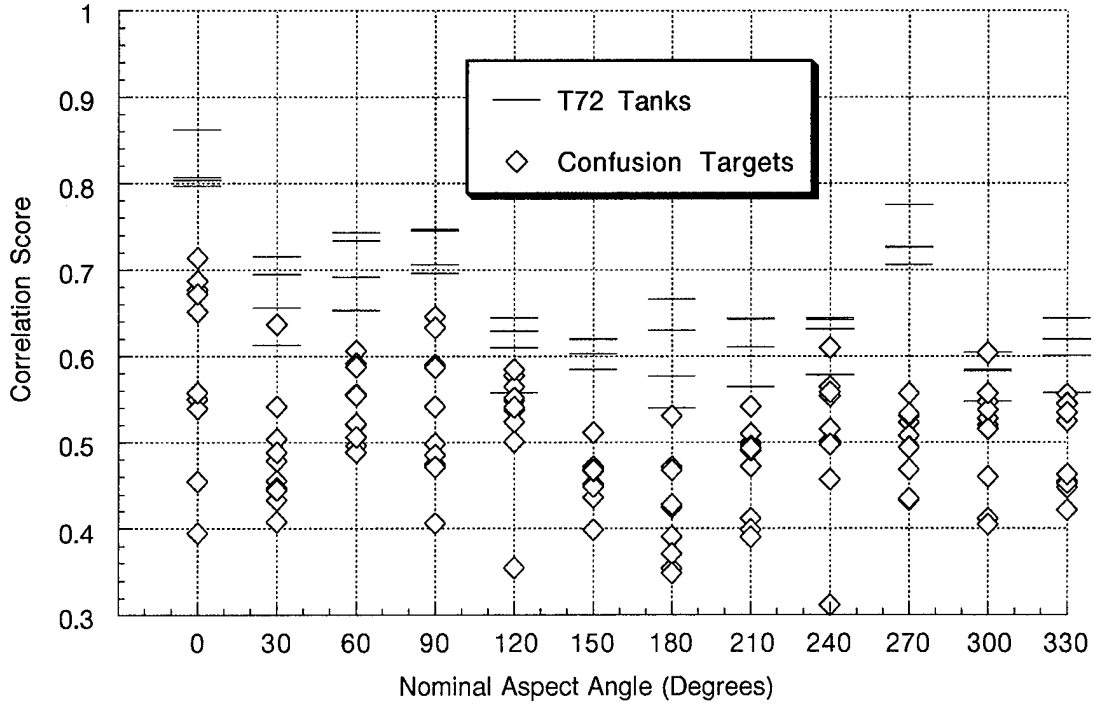

Figure 4-38. Peak Scores for T72-2 SVA Reference Correlation Against All Target Images

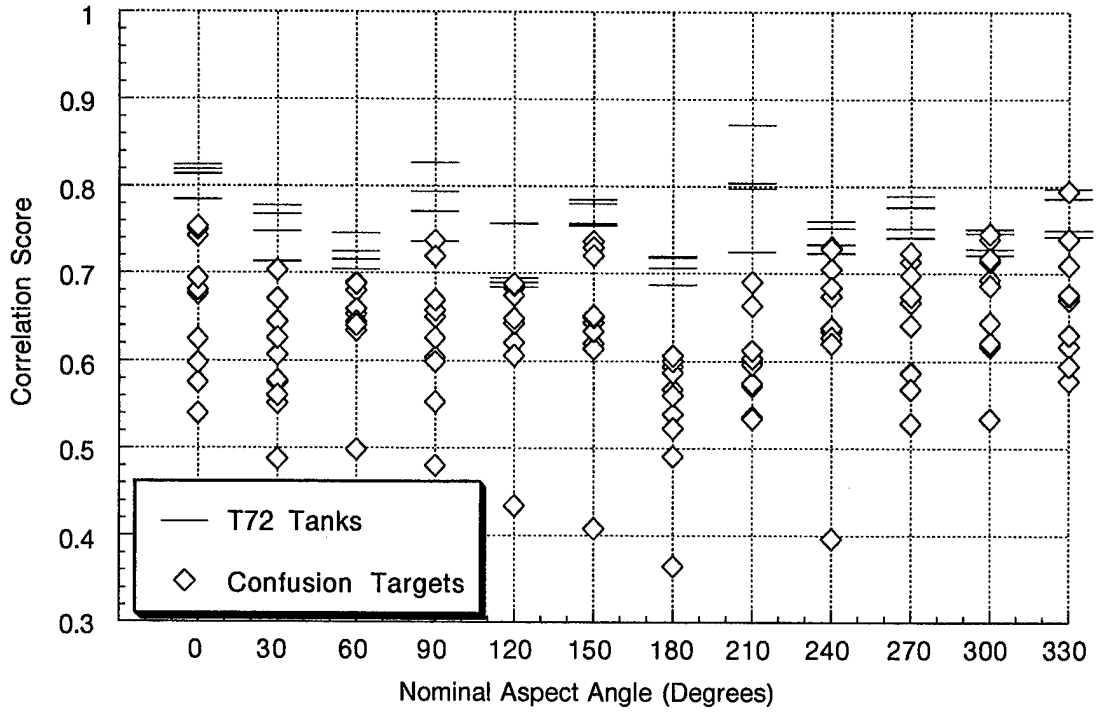

Figure 4-39. Peak Scores for T72-3 TW Reference Correlation Against All Target Images

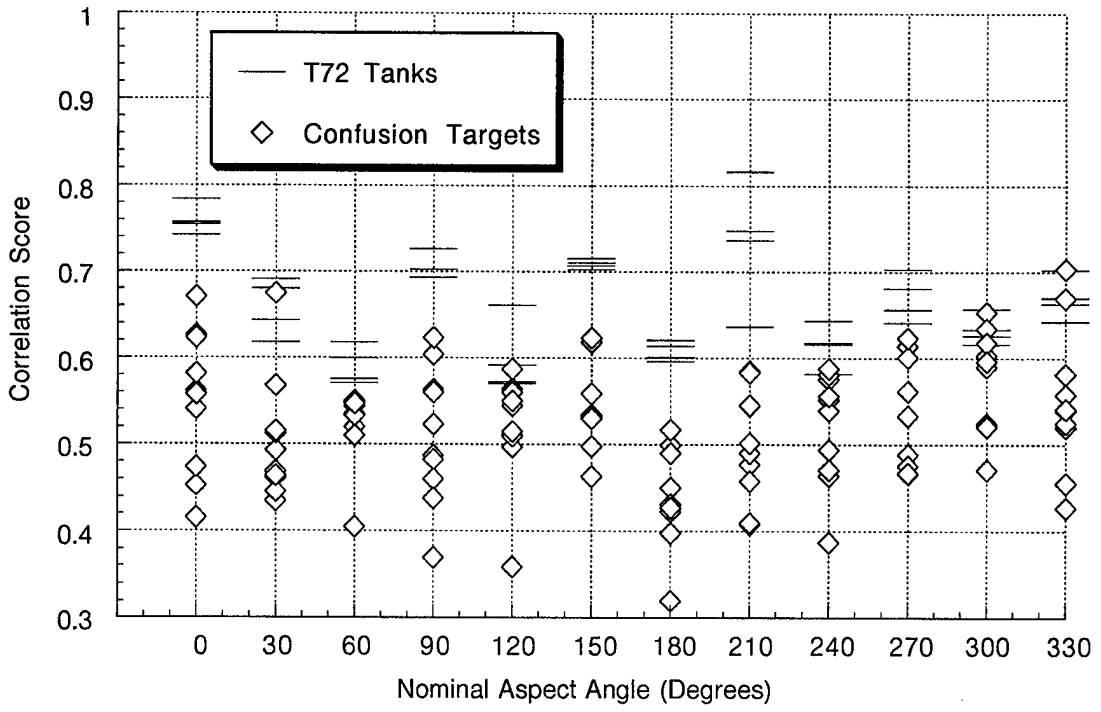

Figure 4-40. Peak Scores for T72-3 SVA Reference Correlation Against All Target Images

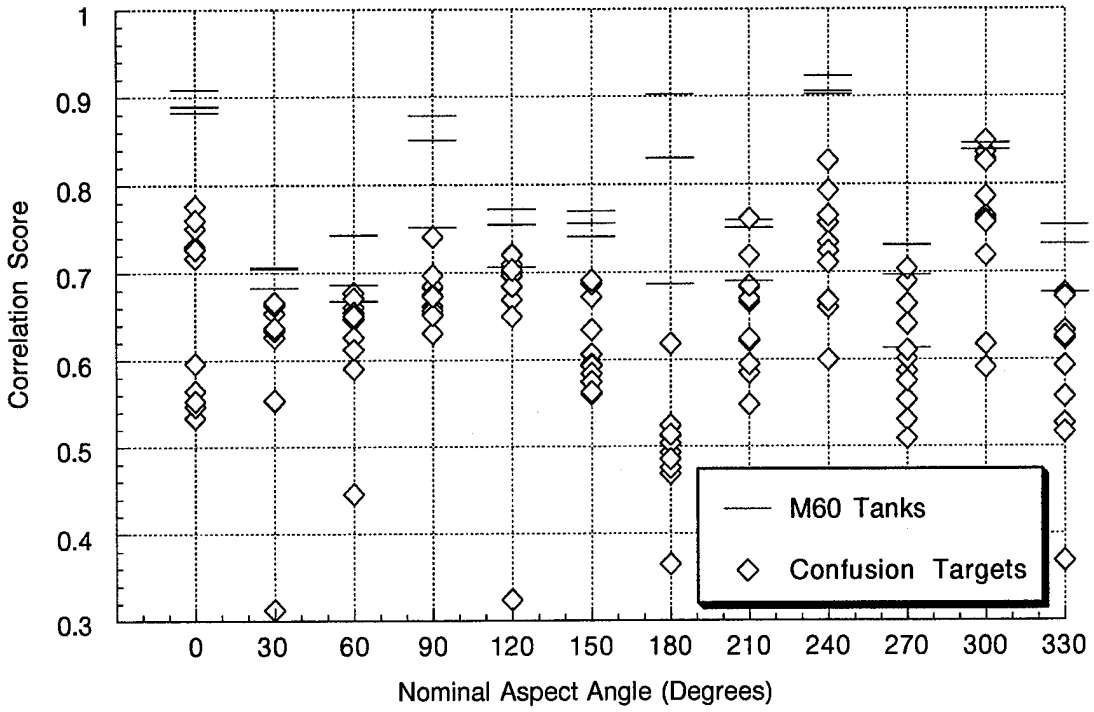

Figure 4-41. Peak Scores for M60-3 TW Reference Correlation Against All Target Images

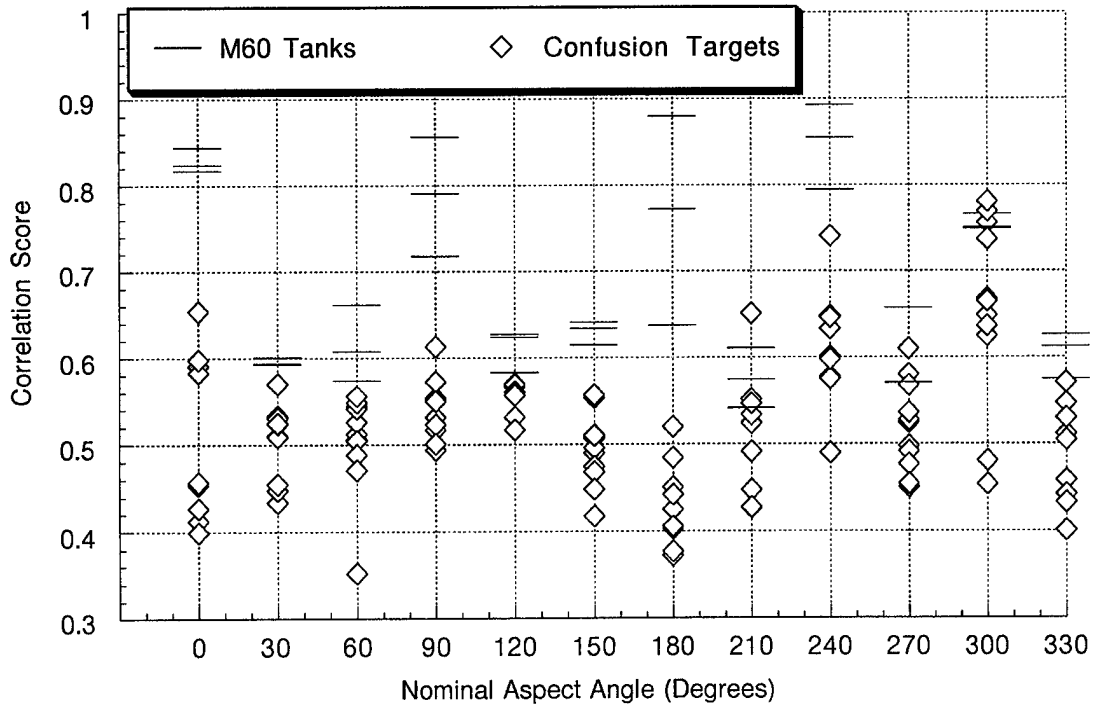

Figure 4-42. Peak Scores for M60-3 SVA Reference Correlation Against All Target Images

Nominal Aspect Angle (Degrees)	TW #MC	SVA #MC	TW Tgt./Conf. Corr. Diff.	SVA Tgt./Conf. Corr. Diff.	Best
0	0	0	0.066	**0.083**	**SVA**
30	**0**	1			**TW**
60	0	0	**0.065**	0.047	**TW**
90	0	0	0.030	**0.050**	**SVA**
120	4	**3**			**SVA**
150	0	0	0.058	**0.073**	**SVA**
180	1	**0**			**SVA**
210	1	**0**			**SVA**
240	1	1			
270	0	0	0.061	**0.149**	**SVA**
300	2	2			
330	2	**0**			**SVA**
Total	**11**	**7**			**8 SVA 2 TW**

Figure 4-43. Best Classification Performance Summary for T72-2 Reference Images

Nominal Aspect Angle (Degrees)	TW #MC	SVA #MC	TW Tgt./Conf. Corr. Diff.	SVA Tgt./Conf. Corr. Diff.	Best
0	0	0	0.032	**0.071**	**SVA**
30	**0**	1			**TW**
60	0	0	0.015	**0.021**	**SVA**
90	1	**0**			**SVA**
120	3	**1**			**SVA**
150	0	0	0.019	**0.079**	**SVA**
180	0	0	**0.081**	0.079	**TW**
210	0	0	0.035	**0.051**	**SVA**
240	2	**1**			**SVA**
270	0	0	0.018	0.018	
300	**2**	3			**TW**
330	**1**	2			**TW**
Total	**9**	**8**			**7 SVA 4 TW**

Figure 4-44. Best Classification Performance Summary for T72-3 Reference Images

Nominal Aspect Angle (Degrees)	TW #MC	SVA #MC	TW Tgt./Conf. Corr. Diff.	SVA Tgt./Conf. Corr. Diff.	Best
0	0	0	0.106	**0.163**	**SVA**
30	0	0	0.017	**0.023**	**SVA**
60	2	**0**			**SVA**
90	0	0	0.011	**1.05**	**SVA**
120	3	**0**			**SVA**
150	0	0	0.050	**0.058**	**SVA**
180	0	0	0.068	**1.17**	**SVA**
210	**2**	3			**TW**
240	0	0	**0.75**	0.054	**TW**
270	4	**2**			**SVA**
300	**1**	3			**TW**
330	0	0	0.001	**0.004**	**SVA**
Total	**12**	**8**			**9 SVA 3 TW**

Figure 4-45. Best Classification Performance Summary for M60-3 Reference Images

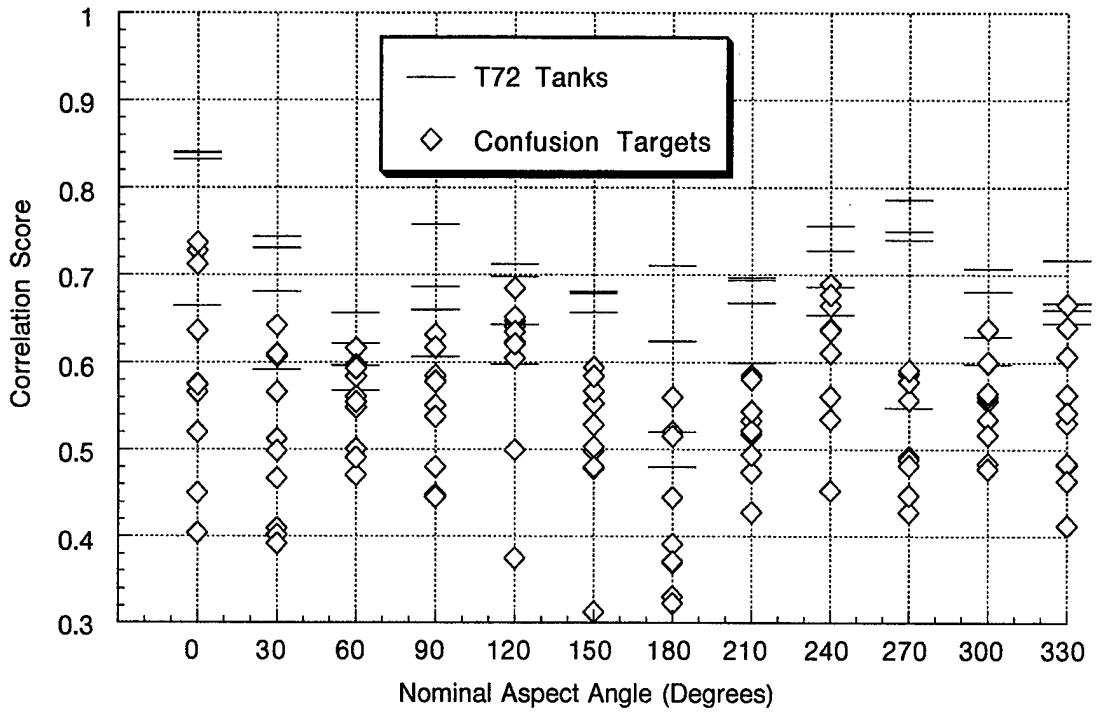

Figure 4-46. Peak Scores for T72-2 TW Reference Correlation Against Target Images at 90 Degree Squint

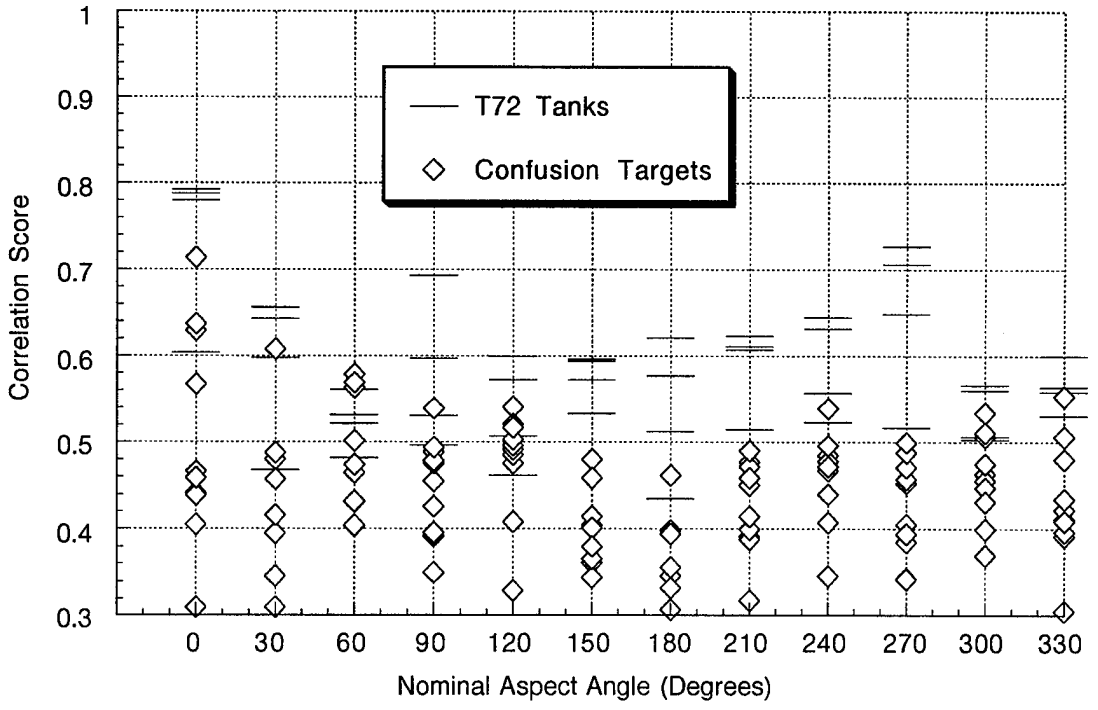

Figure 4-47. Peak Scores for T72-2 SVA Reference Correlation Against Target Images at 90 Degree Squint

5.0 CONCLUSIONS AND RECOMMENDATIONS

The following conclusions can be drawn based on the results of this effort:

- SVA image quality is significantly better than Taylor weighted Fourier image quality for the identical phase history data set. SVA impulse response widths are approximately 25% finer than those of TW imagery, while sidelobe and clutter levels are comparable. SVA image formation processing involves approximately twice the computational burden of traditional Fourier processing.

- ASR image quality is poorer than SVA image quality due to suppression of weak signature components. The relative quality of MVM imagery is difficult to assess, but the computational complexity of the MVM method weighs strongly against its practical utility in any near-term ATR applications.

- SVA imagery offers the potential for improved target classification performance relative to Taylor weighted Fourier imagery. The strength of this conclusion is weakened by the relatively small number of target signatures that were available for analysis. In general, it is believed that the classification advantage of SVA imagery will decrease as intrinsic target variability increases. In the present case, the intrinsic variability of the T72 and M60 tanks was such that SVA demonstrated a limited, positive effect on correlation-based classification performance. In general, it would be expected that the classification performance improvement derived from enhanced image resolution would be obtained at the expense of greater sensitivity to differences in the reference and match target aspect angles.

- The simple correlation-based target classification algorithm performed well in separating tanks of different classes from each other and from other confusion target classes. For each of the three targets selected as reference signatures in this study, 100% correct classification probability was obtained with probability of misclassification equal to 10% or less. Most of the misclassifications, including those for other tank classes, occurred at a few non-cardinal aspect angles.

- Reference target images at aspect angle increments close to 0.5 degrees are required to maintain the performance of the correlation-based classification algorithm. The effect of combining correlation reference images over a wider range of aspect angles was not investigated but, in general, the reduced aspect angle sensitivity attained in that manner would be expected to be offset by a loss of between-class separability (due to reference image blurring).

- The performance of the correlation-based target classification algorithm is very sensitive to small aspect angle differences between the reference and match images. The potential advantages of SVA imagery did not become apparent until sufficient data was analyzed to allow reference and match images to be aligned in aspect to an accuracy of ± 0.25 degrees.

- Intrinsic target variability is a significant factor limiting the performance of the correlation-based classification algorithm. Improved target classification performance might be attained by using a matching algorithm that places more weight on stable portions of the target signatures. Such a procedure may derive increased benefit from SVA processing relative to Taylor weighted Fourier processing, given the increased precision of the stable SVA signature components.

The methodology used in this study should be applied in future SAR ATR development efforts. Separating the effects of intrinsic target variability and small aspect angle mismatches is crucial for developing robust, ATR algorithms. Ideally, target signature data should be obtained for a larger number of target classes and a larger number of different targets within each class. Once classification algorithm performance is understood for targets under the benign deployment conditions, performance sensitivities to other conditions can be systematically investigated. The methodology used in this study could be used in efforts to determine the classification algorithm impact of alternative sensor modalities (polarimetrics and interferometrics), resolutions, and data compression schemes. A simple correlation-based target classification algorithm could be used as a benchmark to judge the effectiveness of more complicated SAR classification algorithms. Finally, future studies should address the effect of alternative classification algorithms that better account for intrinsic target variability.

6.0 REFERENCES

[1] S.I. Stokely, et al., "Three-Dimensional Interferometric Synthetic Aperture Radar (3-D IFSAR) Program," WL-TR-95-1024, February 1995.

[2] S. R. DeGraaf, "SAR Imaging via Modern 2-D Spectral Estimation Methods, Volume I: Imaging Methods Final Report," *ERIM Technical Report 255800-15-F (Vol. I)*, May 1995.

[3] S. R. DeGraaf, "Sidelobe Reduction via Adaptive FIR Filtering in SAR Imagery," *IEEE Trans. on Image Proc.*, Vol. 3, No. 3, May 1994.

[4] S. R. DeGraaf, "SAR Imaging via Modern 2-D Spectral Estimation Methods," *Proc. 1994 SPIE Workshop, Algorithm for Synthetic Aperture Radar,* Orlando, FL, May 1994.

[5] H. C. Stankwitz, R. J. Dallaire, and J. R. Fienup, "Non-Linear Apodization for Sidelobe Control in SAR Imagery," *IEEE Trans. Aerosp. Elec. Sys.*, January 1995.

BLANKET SERVICE ORDER

ERIM 5 1/92

ERIM

COMMUNICATION CENTER/MEDIA PRODUCTION
SERVICE ORDER

ERIM S.O. # Nº 50217

TODAY'S DATE 15 Sep 93 DUE DATE (End of Day) ~~01 Sep 94~~ 3/15/95

An Order With a Due Date Will Take Precedence Over Orders Dated "ASAP" or Left Blank

STATION CODE _____

CMR NO. _____

AUTHOR/ORIGINATOR Stuart DeGraaf EXT. 2800

CONTACT _____ EXT. _____

CHARGE NO. 255850

REPORT NO. 255800 - -L

PROJECT NO. 255800

(When Job Is Completed) AUTHORIZED SIGNER Stuart R. DeGraaf

THIS ORDER AUTHORIZES THE PURCHASE OF ALL MATERIALS AND SERVICES REQUIRED TO COMPLETE THE ORDER

COMMUNICATION CENTER

EDITING: ☐ FORMAT/CONTRACT COMPLIANCE ☐ PUNCTUATION/GRAMMAR ☐ LANGUAGE ☐ ORGANIZATION/ DEVELOPMENT

OTHER (describe): _____

COMPLETED DATE BY

DOCUMENT SERVICES

☐ PROPOSAL
☐ FINAL REPORT
☐ STANDARD ERIM REPORT
☐ PAPER/MEMO
☐ FILE CONVERSION
☐ OTHER

COMPLETED DATE BY
DRAFT
PROOFING
FINAL

GRAPHICS

☐ FIGURES
☐ VIEWGRAPHS
☐ SLIDES
☐ OTHER

ERIM LOGO YES ☐ NO ☐

COMPLETED DATE BY
PROOFING
LEADER APPROVAL

PHOTO

ITEM	QUAN.	

NEW FILE NUMBERS _____

COMPLETED DATE BY

REPRO

137 COPIES OF _____ PAGES, INCLUDING Blue Letterhead COVER (Indicate Color)

☒ REPRODUCE ☒ COLLATE ☒ STAPLE U/L ☐ STAPLE SIDE ☐ TAPE

☐ PUNCH HOLES ☐ ACCO BIND ☐ SPIRAL BIND ☐ INSERT GLOSSY PHOTOS OR OTHER

☐ SPECIAL STOCK REQUIRED: PLEASE INDICATE

OTHER An additional copy of the cover letter will need to be reproduced. Thanks
Plus 1 extra copy of the last page

COMPLETED DATE BY
10/14 DM
11-24 DM
4/27 PT
10/26 DM
10/31-94 DM
11-23-94 DM
4-5-95 DM
11-9-95 DM

DISTRIBUTE ☐ ALL COPIES TO AUTHOR ☐ PER ATTACHED LIST ☒ PER DISTRIBUTION FILES

BLANKET SERVICE ORDER

ERIM 5 1/92

ERIM

COMMUNICATION CENTER/MEDIA PRODUCTION
SERVICE ORDER

ERIM S.O. # Nº 50217

TODAY'S DATE 15 Sep 93 DUE DATE (End of Day) ~~01 Sep 94~~ 3/15/95

STATION CODE _____

CMR NO. _____

An Order With a Due Date Will Take Precedence Over Orders Dated "ASAP" or Left Blank

AUTHOR/ORIGINATOR Stuart DeGraaf EXT. 2800

CONTACT _____ EXT. _____

CHARGE NO. 255850

REPORT NO. 255800 - -L

PROJECT NO. 255800

(When Job Is Completed) AUTHORIZED SIGNER Stuart R. DeGraaf

THIS ORDER AUTHORIZES THE PURCHASE OF ALL MATERIALS AND SERVICES REQUIRED TO COMPLETE THE ORDER

COMMUNICATION CENTER

EDITING: ☐ FORMAT/CONTRACT COMPLIANCE ☐ PUNCTUATION/GRAMMAR ☐ LANGUAGE ☐ ORGANIZATION/ DEVELOPMENT

OTHER (describe): _____

COMPLETED DATE BY

DOCUMENT SERVICES

☐ PROPOSAL
☐ FINAL REPORT
☐ STANDARD ERIM REPORT
☐ PAPER/MEMO
☐ FILE CONVERSION
☐ OTHER

COMPLETED DATE BY
DRAFT
PROOFING
FINAL

GRAPHICS

☐ FIGURES
☐ VIEWGRAPHS
☐ SLIDES
☐ OTHER

ERIM LOGO YES ☐ NO ☐

COMPLETED DATE BY
PROOFING
LEADER APPROVAL

PHOTO

ITEM	QUAN.	

NEW FILE NUMBERS _____

COMPLETED DATE BY

REPRO

137 COPIES OF _____ PAGES, INCLUDING Blue Letterhead COVER (Indicate Color)

☒ REPRODUCE ☒ COLLATE ☒ STAPLE U/L ☐ STAPLE SIDE ☐ TAPE

☐ PUNCH HOLES ☐ ACCO BIND ☐ SPIRAL BIND ☐ INSERT GLOSSY PHOTOS OR OTHER

☐ SPECIAL STOCK REQUIRED: PLEASE INDICATE

OTHER An additional copy of the cover letter will need to be reproduced. Thanks Plus 1 extra copy of the last page

COMPLETED DATE BY
10/19 DM
11-24 DM
4/27 PT
10/26- DM
10/31-94 DM
11-23-94 DM
4-5-95 DC
11-9-95 DM

DISTRIBUTE ☐ ALL COPIES TO AUTHOR ☐ PER ATTACHED LIST ☒ PER DISTRIBUTION FILES